



Strong constraints on the $b \rightarrow s\gamma$ photon polarisation from $B^0 \rightarrow K^{*0}e^+e^-$ decays

LHCb collaboration[†]

Abstract

An angular analysis of the $B^0 \rightarrow K^{*0}e^+e^-$ decay is performed using a data sample corresponding to an integrated luminosity of 9 fb^{-1} of pp collisions collected with the LHCb experiment. The analysis is conducted in the very low dielectron mass squared (q^2) interval between 0.0008 and 0.257 GeV^2 , where the rate is dominated by the $B^0 \rightarrow K^{*0}\gamma$ transition with a virtual photon. The fraction of longitudinal polarisation of the K^{*0} meson, F_L , is measured to be $F_L = (4.4 \pm 2.6 \pm 1.4)\%$, where the first uncertainty is statistical and the second systematic. The A_T^{Re} observable, which is related to the lepton forward-backward asymmetry, is measured to be $A_T^{\text{Re}} = -0.06 \pm 0.08 \pm 0.02$. The $A_T^{(2)}$ and A_T^{Im} transverse asymmetries, which are sensitive to the virtual photon polarisation, are found to be $A_T^{(2)} = 0.11 \pm 0.10 \pm 0.02$ and $A_T^{\text{Im}} = 0.02 \pm 0.10 \pm 0.01$. The results are consistent with Standard Model predictions and provide the world's best constraint on the $b \rightarrow s\gamma$ photon polarisation.

Published in JHEP **12** (2020) 081

© 2022 CERN for the benefit of the LHCb collaboration. CC BY 4.0 licence.

[†]Authors are listed at the end of this paper.

1 Introduction

Decay processes mediated by $b \rightarrow s\gamma$ transitions are suppressed in the Standard Model (SM) as they proceed through flavour-changing neutral currents involving electroweak-loop Feynman diagrams. The precise study of their properties is sensitive to small contributions from physics beyond the Standard Model (BSM). Since in the SM the weak force only couples to left-handed quarks, the photons emitted in $b \rightarrow s\gamma$ transitions are predominantly left-handed. The contribution with right-handed polarisation is suppressed by the ratio of the s and b quark masses. Therefore, a larger right-handed contribution would represent a clear sign of BSM physics [1–10]. The chirality of the $b \rightarrow s\gamma$ transition was indirectly probed at the BaBar, Belle and LHCb experiments, using measurements of the inclusive $B \rightarrow X_s\gamma$ branching ratio [11–15] as well as the mixing-induced CP asymmetries and time-dependent decay rates of radiative B^0 and B_s^0 decays [16–18]. In this paper, the $b \rightarrow s\ell\ell$ transition where the dilepton pair originates from a virtual photon is used to measure the $b \rightarrow s\gamma$ photon polarisation. In order to isolate $b \rightarrow s\ell^+\ell^-$ transitions dominated by the $b \rightarrow s\gamma$ contribution, the analysis is restricted to a region of very low dilepton mass squared (q^2), which can only be accessed via the $b \rightarrow se^+e^-$ transition due to the low electron mass [19, 20]. This paper presents an angular analysis of the $B^0 \rightarrow K^{*0}e^+e^-$ decay¹ in the region of q^2 between 0.0008 and 0.257 GeV². The symbol K^{*0} denotes the $K^{*0}(892)$ meson reconstructed via its decay $K^{*0} \rightarrow K^+\pi^-$. An angular analysis of $B^0 \rightarrow K^{*0}e^+e^-$ decays was performed by LHCb in the q^2 region between 0.002 and 1.120 GeV² [21]. The analysis presented here uses a data sample collected between the years 2011 and 2018. This sample comprises approximately five times as many B^0 decays. This analysis also employs a selection technique that greatly improves the signal purity as well as the sensitivity to the $b \rightarrow s\gamma$ photon polarisation.

The $B^0 \rightarrow K^{*0}e^+e^-$ decay can be described over the full q^2 range by the left (right)-handed Wilson coefficients $C_7^{(\prime)}$, $C_9^{(\prime)}$ and $C_{10}^{(\prime)}$ [22, 23]. These coefficients encode information about short-distance effects and are sensitive to BSM physics. The detailed description of the $B^0 \rightarrow K^{*0}\ell^+\ell^-$ differential decay rate involves hadronic form factors describing the $B^0 \rightarrow K^{*0}$ transition and other long-distance effects that can be difficult to predict [24–27]. The results of the angular analysis of the $B^0 \rightarrow K^{*0}\mu^+\mu^-$ decay [28], the measurements of the branching fractions of several $b \rightarrow s\ell^+\ell^-$ decays [29–31] and the ratio of the branching fractions of the electron and muon channels of $B^0 \rightarrow K^{*0}\ell^+\ell^-$ and $B^+ \rightarrow K^+\ell^+\ell^-$ decays [32, 33] exhibit tensions with respect to SM predictions. Model independent fits of the $b \rightarrow s\ell^+\ell^-$ measurements involve all of the Wilson coefficients mentioned above [34–38]. Since the very-low- q^2 region is associated with the left- and right-handed electromagnetic operators [19], it contains unique information that can be used to determine the C_7 and C_7' Wilson coefficients.

For the $B^0 \rightarrow K^{*0}e^+e^-$ decay the partial decay width can be described in terms of q^2 and three angles θ_ℓ , θ_K and ϕ . The angle θ_ℓ is defined as the angle between the direction of the e^+ and the direction opposite to that of the B^0 meson in the dielectron rest frame. The angle θ_K is defined as the angle between the direction of the kaon and the direction opposite to that of the B^0 meson in the K^{*0} meson rest frame. The angle ϕ is the angle between the plane containing the electron and positron and the plane containing the kaon and pion in the B^0 meson rest frame. The basis is chosen so that the angular definition for

¹The inclusion of charge-conjugate processes is implied throughout this paper. Natural units with $c = 1$ are used throughout this paper.

the \bar{B}^0 decay is the CP conjugate of that of the B^0 decay. These definitions are identical to those used for the $B^0 \rightarrow K^{*0} \mu^+ \mu^-$ analysis in Ref. [39], including the sign flip of ϕ ($\phi \rightarrow -\phi$) for the \bar{B}^0 decay. The angle ϕ is transformed such that $\tilde{\phi} = \phi + \pi$ if $\phi < 0$. This transformation cancels out terms that have a $\sin \phi$ or $\cos \phi$ dependence and simplifies the angular expression without any loss of sensitivity to the remaining observables. In the region of q^2 considered in this paper, where the photon is almost on-shell, the fraction of $K^+ \pi^-$ pairs in an S-wave configuration is suppressed with respect to the value measured at higher q^2 [40], because a longitudinally polarised $K^+ \pi^-$ pair cannot couple to a real photon. Using Refs. [41, 42] it can be shown that the ratio of the S-wave fraction to the fraction of longitudinal polarisation of the K^{*0} is constant as function of q^2 in the 0-6 GeV² range. Neglecting the $K^+ \pi^-$ S-wave contribution, and in the limit of massless leptons (a very good approximation for electrons), the $B^0 \rightarrow K^{*0} e^+ e^-$ angular distribution can be expressed as

$$\begin{aligned} \frac{1}{d(\Gamma + \bar{\Gamma})/dq^2} \frac{d^4(\Gamma + \bar{\Gamma})}{dq^2 d\cos\theta_\ell d\cos\theta_K d\tilde{\phi}} &= \frac{9}{16\pi} \left[\frac{3}{4}(1 - F_L) \sin^2 \theta_K + F_L \cos^2 \theta_K \right. \\ &+ \frac{1}{4}(1 - F_L) \sin^2 \theta_K \cos 2\theta_\ell - F_L \cos^2 \theta_K \cos 2\theta_\ell \\ &+ (1 - F_L) A_T^{\text{Re}} \sin^2 \theta_K \cos \theta_\ell \\ &+ \frac{1}{2}(1 - F_L) A_T^{(2)} \sin^2 \theta_K \sin^2 \theta_\ell \cos 2\tilde{\phi} \\ &\left. + \frac{1}{2}(1 - F_L) A_T^{\text{Im}} \sin^2 \theta_K \sin^2 \theta_\ell \sin 2\tilde{\phi} \right]. \end{aligned} \quad (1)$$

The four angular observables F_L , A_T^{Re} , $A_T^{(2)}$ and A_T^{Im} are combinations of the transversity amplitudes A_0 , A_\perp and A_\parallel , as detailed in Ref. [21]. The observable F_L corresponds to the longitudinal polarisation fraction of the K^{*0} meson and is expected to be small at low q^2 , since the virtual photon is quasi-real and therefore transversely polarised. The observable A_T^{Re} is related to the lepton forward-backward asymmetry, A_{FB} , by $A_T^{\text{Re}} = \frac{4}{3} A_{\text{FB}}(1 - F_L)$ [43]. The observable $A_T^{(2)}$ is averaged between B^0 and \bar{B}^0 decays, while, given the ϕ sign flip for \bar{B}^0 decays, A_T^{Im} corresponds to a CP asymmetry [44]. The A_T^{Re} , $A_T^{(2)}$ and A_T^{Im} transverse asymmetries are related to the P_i angular basis [45] through $A_T^{\text{Re}} = 2P_2$, $A_T^{(2)} = P_1$ and $A_T^{\text{Im}} = -2P_3^{CP}$.

The $A_T^{(2)}$ and A_T^{Im} observables depend only on the $B^0 \rightarrow K^{*0} e^+ e^-$ transversity amplitudes, A_\perp and A_\parallel , and vanish if these amplitudes are completely left-handed. In the limit $q^2 \rightarrow 0$, which is a good approximation for the q^2 region considered in this paper, the $A_T^{(2)}$ and A_T^{Im} observables are closely related to the photon polarisation in $B^0 \rightarrow K^{*0} \gamma$ transitions. In particular, the ratio of the right- and left-handed photon amplitudes, A_R and A_L , can be related to $A_T^{(2)}$ and A_T^{Im} through [10, 43]

$$\begin{aligned} \tan \chi &\equiv |A_R/A_L|, \\ A_T^{(2)} &= \sin(2\chi) \cos(\phi_L - \phi_R), \\ A_T^{\text{Im}} &= \sin(2\chi) \sin(\phi_L - \phi_R), \end{aligned} \quad (2)$$

where $\phi_{L(R)}$ is the $A_{L(R)}$ weak phase and the small strong phase difference between the amplitudes is neglected. Corrections to these approximations, due to terms proportional

to C_9 and C_{10} , are smaller than 0.006 even in the presence of large BSM effects in $C_7^{(\prime)}$ [46]. The mixing-induced CP asymmetries and time-dependent decay rates of radiative B^0 and B_s^0 decays have very similar expressions, but also involve B -mixing phases [10].

The $A_T^{(2)}$ and A_T^{Im} observables are predicted to be very small in the SM when compared to the current experimental sensitivity. Using the FLAVIO software package [46] (version 2.0.0) the following SM predictions are calculated for the four angular observables in the q^2 range considered

$$\begin{aligned}
 F_L(\text{SM}) &= 0.051 \pm 0.013, \\
 A_T^{\text{Re}}(\text{SM}) &= -0.0001 \pm 0.0004, \\
 A_T^{(2)}(\text{SM}) &= 0.033 \pm 0.020, \\
 A_T^{\text{Im}}(\text{SM}) &= -0.00012 \pm 0.00034.
 \end{aligned}
 \tag{3}$$

A detailed discussion of the theoretical uncertainties on the hadronic contributions involved in these predictions can be found in Ref. [10]. The uncertainties on the transverse asymmetries are much smaller than the experimental sensitivity of the results presented in this paper.

2 The LHCb detector and data set

The study reported here is based on pp collision data, corresponding to an integrated luminosity of 9 fb^{-1} , collected at the Large Hadron Collider (LHC) with the LHCb detector [47]. The data were taken in the years 2011, 2012 and 2015–2018, at centre-of-mass energies of 7, 8 and 13 TeV, respectively. The LHCb detector [47, 48] is a single-arm forward spectrometer covering the pseudorapidity range $2 < \eta < 5$. The detector includes a tracking system consisting of a vertex detector surrounding the pp interaction region and of tracking stations on either sides of a 4 Tm dipole magnet. Charged particles are identified using information from two ring-imaging Cherenkov detectors (RICH), electromagnetic (ECAL) and hadronic (HCAL) calorimeters and muon chambers. The online event selection is performed by a trigger, which consists of a hardware stage, based on information from the calorimeters and muon system, followed by a software stage, which fully reconstructs the event. The hardware electron trigger requires the presence of an ECAL cluster with minimum transverse energy between 2.5 and 3.0 GeV, depending on the data-taking period. Signal $B^0 \rightarrow K^{*0} e^+ e^-$ candidates are retained if at least one of the electrons fires the electron trigger. Alternatively, candidates are selected if the hardware trigger requirements were passed by objects in the rest of the event that are independent of the decay products of the signal B^0 candidate. The software trigger requires a two-, three- or four-track vertex with a significant displacement from a primary pp interaction vertex (PV). At least one charged particle must have a significant transverse momentum (p_T) and be inconsistent with originating from any PV. A multivariate algorithm [49] is used to identify displaced vertices consistent with the decay of a b hadron.

Samples of simulated events, produced with the software described in Refs. [50–55], are used to characterise signal and background contributions. The simulated samples are corrected for known differences between data and simulation in kinematics, particle identification, detector occupancy, hardware trigger efficiency and reconstruction effects, based on a general approach developed by the LHCb collaboration for tests of lepton universality [33].

3 Reconstruction and selection

The $B^0 \rightarrow K^{*0}e^+e^-$ candidates are formed by combining a K^{*0} candidate with a pair of oppositely charged tracks identified as electrons. For events passing the trigger, K^{*0} candidates are formed by combining a pair of charged tracks identified as K^+ and π^- mesons. Each track is required to be of good quality and to be inconsistent with originating from a PV. Kaons and pions are required to have transverse momenta larger than 250 MeV and are identified using information from the RICH detectors. Electrons with p_T exceeding 500 MeV and with a good-quality vertex are used to form dielectron candidates. The reconstructed invariant mass of the $K^+\pi^-$ system is required to be within 100 MeV of the mass of the K^{*0} meson [56].

The tracks from the electrons, kaon and pion are required to form a good-quality vertex that is significantly displaced from any PV. In events with multiple PVs, the one with the smallest value of χ_{IP}^2 is associated to the $B^0 \rightarrow K^{*0}e^+e^-$ candidate. Here χ_{IP}^2 is defined as the difference in the vertex-fit χ^2 of a given PV reconstructed with and without the tracks forming the candidate under consideration. In addition, the angle between the B^0 -candidate momentum vector and the vector between the associated PV and the B^0 decay vertex is required to be small.

Electrons can lose a significant amount of their energy when interacting with the detector material due to emission of bremsstrahlung photons. A dedicated procedure, which searches for neutral energy deposits in the ECAL that are compatible with being emitted by the electron upstream of the magnet, is applied to correct for this effect [33]. The limitations of this recovery technique degrade the resolution of the reconstructed invariant masses of both the dielectron pair and the B^0 candidate.

4 Analysis strategy

The q^2 region under study is chosen to maximise the sensitivity to $b \rightarrow s\gamma$ contributions ($C_7^{(\prime)}$). First of all, the reconstructed invariant-mass squared resolution of the dielectron pair is improved by a kinematic fit that constrains the $K^+\pi^-e^+e^-$ mass to the known B^0 mass [56]. The reconstructed q^2 is required to be lower than 0.25 GeV^2 to minimise the sensitivity to vector and axial-vector currents ($C_9^{(\prime)}$ and $C_{10}^{(\prime)}$) while retaining as many signal candidates as possible. The larger data set of this analysis makes it possible to significantly reduce this upper bound with respect to Ref. [21], where it was 1 GeV^2 . Low- q^2 signal candidates are most sensitive to $C_7^{(\prime)}$, but suffer from a degradation of the resolution in $\tilde{\phi}$ due to multiple scattering of the quasi-collinear electrons in the tracking detectors. Furthermore, $B^0 \rightarrow K^{*0}\gamma$ decays followed by a photon conversion in the material of the detector contaminate the lower end of the q^2 spectrum. The reconstructed q^2 is thus required to exceed 10^{-4} GeV^2 , resulting in a $\tilde{\phi}$ resolution of 0.11 rad and a $B^0 \rightarrow K^{*0}\gamma$ background fraction of about 2% (see Sec. 5).

The signal selection efficiency as a function of the dielectron mass, obtained from simulation, is presented in Fig. 1. The efficiency is approximately uniform across the signal region. Close to the boundaries, the efficiency drops due to the selected range of reconstructed q^2 and the effect of the dielectron mass resolution. Therefore, following Ref. [21], effective q^2 boundaries are defined between 0.0008 GeV^2 and 0.257 GeV^2 to allow for theoretical predictions of the angular observables without input from LHCb simulation.

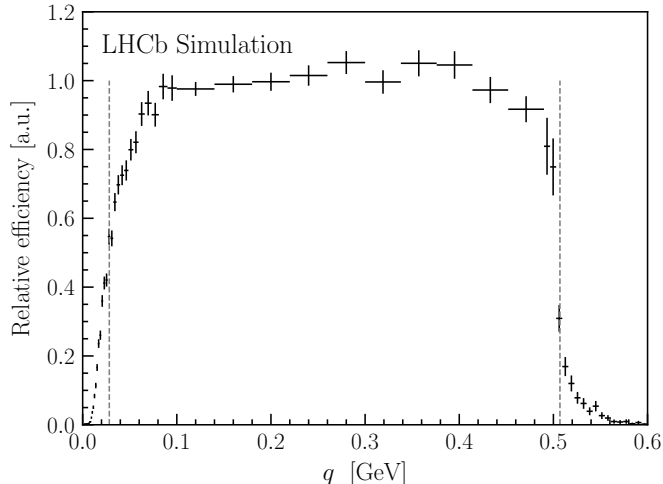


Figure 1: Relative efficiency as a function of the dielectron invariant mass (q). The points represent the efficiency obtained from simulation, while the vertical lines represent the effective q^2 boundary defined in the text.

Using the FLAVIO software package, it was checked that predictions with both SM and BSM values for the Wilson coefficients calculated in this effective q^2 range (grey line in Fig. 1) agree very well with those calculated taking into account a complete description of the q^2 efficiency using LHCb simulation (points in Fig. 1).

The region of reconstructed q^2 below 10^{-4} GeV^2 is enriched in $B^0 \rightarrow K^{*0} \gamma$ decays and is used as a control sample. Its kinematics and background level are very similar to the signal q^2 region, but with much larger candidate yields.

The $B^0 \rightarrow K^{*0} e^+ e^-$ branching ratio is expected to be as small as $(2.0 \pm 0.4) \times 10^{-7}$ in the q^2 range studied in this paper [46]. Nonetheless, a pure signal sample is obtained by greatly reducing all expected background contributions with the selection described in Sec. 5. A fit to the reconstructed $K^{*0} e^+ e^-$ invariant mass, $m(K^+ \pi^- e^+ e^-)$, in a wide range between 4500 and 6200 MeV is used to estimate the remaining background contamination, as explained in Sec. 6. Afterwards, a four-dimensional fit to the $K^+ \pi^- e^+ e^-$ invariant mass and the three angles $\cos \theta_\ell$, $\cos \theta_K$ and $\hat{\phi}$ is used to measure the four angular observables F_L , A_T^{Re} , $A_T^{(2)}$ and A_T^{Im} . This fit is performed in a reduced $m(K^+ \pi^- e^+ e^-)$ window between 5000 and 5400 MeV in order to simplify the angular modelling of the background components. The background fractions are constrained to those obtained in the wider $m(K^+ \pi^- e^+ e^-)$ window. Signal and background angular shapes are determined using simulation and data samples (Sec. 7) and then fitted to the signal sample (Sec. 8).

The $m(K^+ \pi^- e^+ e^-)$ mass resolution, the angular acceptance and the background rates depend on how the event has been triggered at the hardware level. The data sample is therefore divided into two categories: events for which at least one of the two electron candidates fires the electron trigger, and events triggered by activity in the event that is not associated with any of the signal decay particles. Furthermore, the data sets collected in 2011–12 (Run 1) and 2015–18 (Run 2) are treated separately to account for kinematic differences due to the different pp collision energies.

5 Background studies

Several sources of specific background are considered, with studies performed using samples of simulated events unless stated otherwise. All of the identified background sources that are expected to contribute at a level of more than 1% of the signal are modelled and included in the analysis.

A large background comes from the semileptonic $B^0 \rightarrow D^- e^+ \nu$ decay, with $D^- \rightarrow K^{*0} e^- \bar{\nu}$. This contribution populates the region below the B^0 mass and has a combined branching fraction four orders of magnitude larger than that of the signal. In the case where both neutrinos have low energies, the signal selection is ineffective at rejecting it. The positron from the B^0 decay tends to be more energetic than the electron from the D^- decay and hence the reconstructed $\cos \theta_\ell$ distribution favours large values since $\cos \theta_\ell$ is highly correlated with the $e^+ e^-$ energy asymmetry. In order to avoid any potential bias in the measurement of A_T^{Re} , a symmetric requirement of $|\cos \theta_\ell| < 0.8$ is applied, resulting in a 5% loss of signal while rejecting 98% of this semileptonic background.

The radiative decay $B^0 \rightarrow K^{*0} \gamma$ has a branching fraction about two orders of magnitude larger than that of the signal and has a very similar distribution in the reconstructed $K^+ \pi^- e^+ e^-$ mass. In the signal sample, contamination from this background is at the level of 23%, but is reduced to about 2% by rejecting dielectron pairs compatible with originating from detector material [57]. A specific weighting procedure is applied to the $B^0 \rightarrow K^{*0} \gamma$ simulation to match the true $e^+ e^-$ mass distribution of Ref. [58] since the GEANT4 version used here does not accurately model high-mass $e^+ e^-$ pair production.

The $B^0 \rightarrow K^{*0} \eta$ and $B^0 \rightarrow K^{*0} \pi^0$ decays where the η or π^0 meson decays to $e^+ e^- \gamma$ (Dalitz decay) can pass the selection if the photon is very soft, or if it is recovered as a bremsstrahlung photon. In the latter case, the $m(K^+ \pi^- e^+ e^-)$ mass peaks at the B^0 mass. The contamination from the η (π^0) Dalitz decay is estimated to be at the level of 4% (2%) in the mass region used in the angular fit.

To suppress background from $B_s^0 \rightarrow \phi e^+ e^-$ decays, where the ϕ meson decays to a $K^+ K^-$ pair and one of the kaons is misidentified as a pion, the two-hadron invariant mass computed under the $K^+ K^-$ hypothesis is required to be larger than 1040 MeV. Background contributions from misidentified $\Lambda_b^0 \rightarrow p K^- e^+ e^-$, $B^0 \rightarrow K^{*0} \pi^+ \pi^-$ and $\bar{B}^0 \rightarrow \bar{K}^{*0} e^+ e^-$ decays are found to be negligible.

Partially reconstructed (PR) background contributions arising from $B \rightarrow K^{*0} \pi e^+ e^-$ decays, where one of the pions is not reconstructed, are suppressed by exploiting the kinematic balance of the decay. The ratio of the K^{*0} and dielectron momenta components transverse to the B^0 direction is expected to be unity unless some energy is lost through bremsstrahlung emission. Since at low q^2 bremsstrahlung photons do not significantly modify the dielectron direction, this ratio can be used to recover the lost energy and recompute the corrected reconstructed B^0 mass called m_{HOP} [33]. In the case of PR background, however, the missing particles are not necessarily emitted in the same direction as either electron. Therefore the requirement $m_{\text{HOP}} > 4900$ MeV rejects about 70% of the PR background with a 90% signal efficiency, estimated from simulation. This background yield is found to be 5% of that of the signal in the narrow mass window.

In order to reduce the level of combinatorial background, a multivariate classifier based on a boosted decision tree algorithm (BDT) [59, 60] is used. The BDT classifier is trained to separate simulated $B^0 \rightarrow K^{*0} e^+ e^-$ events from background events taken from the upper invariant-mass sideband ($m(K^+ \pi^- e^+ e^-) > 5600$ MeV) in data and uses eight kinematic

and decay topology variables including the χ_{IP}^2 of final-state particles with respect to the associated PV and the p_{T} of the B^0 candidate and its flight distance from the PV. The classifier achieves a background rejection of 90% and a signal efficiency of 94%. The semileptonic and combinatorial background sources contribute a contamination of about 7% and are therefore modelled in the fit to the data.

6 $K^+\pi^-e^+e^-$ invariant-mass spectra

An unbinned maximum-likelihood fit to the $K^+\pi^-e^+e^-$ invariant-mass distribution is performed simultaneously to the signal and control samples in order to measure the background fractions. In both samples, the $B^0 \rightarrow K^{*0}e^+e^-$ and $B^0 \rightarrow K^{*0}\gamma$ components are described by a bifurcated Crystal Ball (CB) function [61], which consists of a Gaussian core with asymmetric power-law tails. The shapes of the $K^{*0}\eta$ and $K^{*0}\pi^0$ background contributions are modelled by non-parametric probability density functions (PDFs) [62], while the shape of the PR background is modelled by the sum of a CB function and a Gaussian function. Finally, the shapes of the semileptonic and combinatorial background (SL/C) are parametrised together by an exponential function. All shapes apart from the SL/C are fixed from simulation. The widths and mean values of the signal CB functions are corrected for differences between data and simulation using a high-purity data sample of $B^0 \rightarrow J/\psi(e^+e^-)K^{*0}$ candidates.

Since the $b \rightarrow s\gamma$ contribution dominates both the $B^0 \rightarrow K^{*0}e^+e^-$ and $B \rightarrow K^{*0}\pi^+e^-$ decay rates in the q^2 region considered, the PR background is expected to be similar for the signal and control samples. The ratio of PR background and signal yields is therefore shared between the two samples. Using the fit in the wider $m(K^+\pi^-e^+e^-)$ mass window, the $B^0 \rightarrow K^{*0}e^+e^-$ yield in the restricted $m(K^+\pi^-e^+e^-)$ range used for the angular fit is estimated to be 450. In the control sample, the $B^0 \rightarrow K^{*0}\gamma$ yield is about 2950, while in both samples the signal-to-background ratio is about 5. The invariant-mass distributions together with the PDFs resulting from the fit are shown in Figs. 2 and 3 for the control and signal samples, respectively.

7 Angular modelling

The $B^0 \rightarrow K^{*0}e^+e^-$ angular distribution described using Eq. 1 is multiplied by an acceptance function evaluated from simulated $B^0 \rightarrow K^{*0}e^+e^-$ decays to take into account the effect of the reconstruction and selection efficiency. The acceptance function, ε , factorises between the angles such that

$$\varepsilon(\cos\theta_\ell, \cos\theta_K, \tilde{\phi}) \simeq \varepsilon(\cos\theta_\ell)\varepsilon(\cos\theta_K)\varepsilon(\tilde{\phi}). \quad (4)$$

The $\cos\theta_K$ and $\cos\theta_\ell$ acceptance functions are modelled with fourth-order Legendre polynomials. For the $\tilde{\phi}$ angle, non-uniform acceptance terms proportional to $\cos(2\tilde{\phi})$ and $\sin(2\tilde{\phi})$ are allowed for completeness, however, no significant deviation from a uniform distribution is observed.

Since for $B^0 \rightarrow K^{*0}\gamma$ decays the presence of the electrons is only due to the interaction of the real photon with the detector material, the $\cos\theta_\ell$ and $\tilde{\phi}$ dependent parts of Eq. 1 are integrated out to model purely the $\cos\theta_K$ dependent part of the $B^0 \rightarrow K^{*0}\gamma$ angular

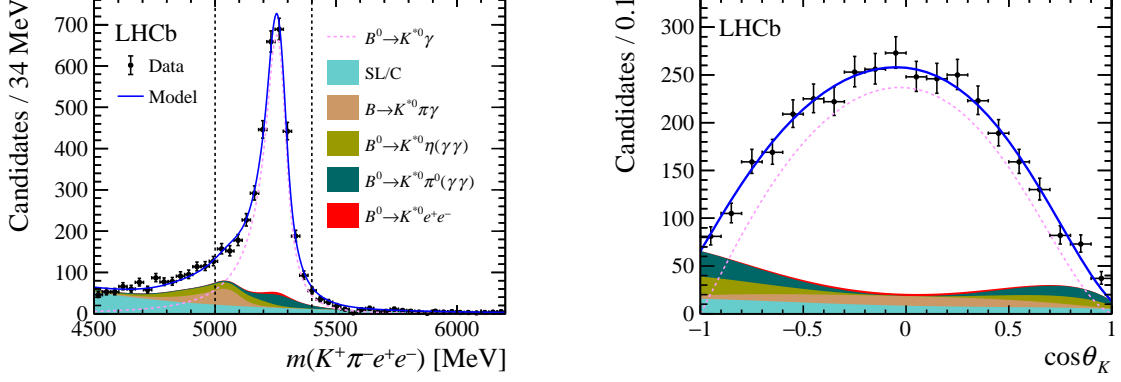


Figure 2: Distributions of the (left) $K^+\pi^-e^+e^-$ invariant mass and (right) $\cos\theta_K$ of $B^0 \rightarrow K^{*0}\gamma$ candidates. The black points represent the data, while the solid blue curve shows the total PDF. The signal component is represented by the dashed pink line and the shaded areas are the background components, as detailed in the legend. The SL/C component is composed of semileptonic and combinatorial background contributions. The dashed vertical lines indicate the restricted mass range used in the angular analysis.

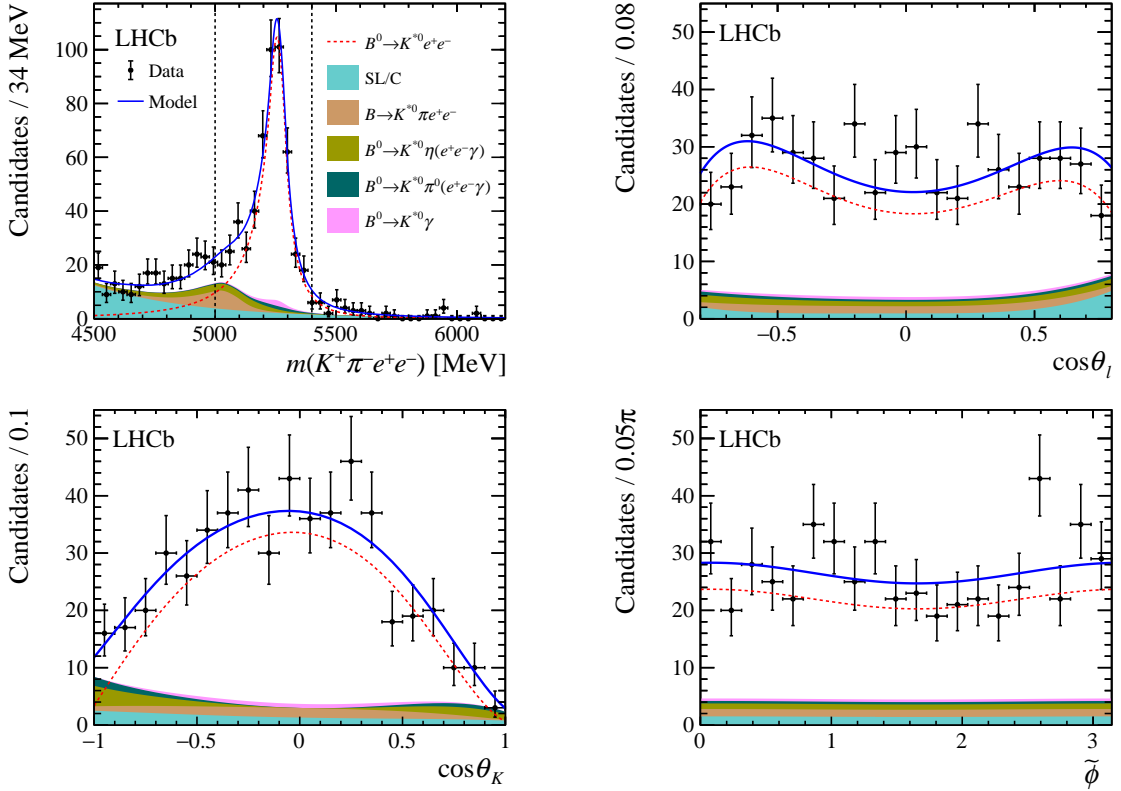


Figure 3: Distributions of the (top left) $K^+\pi^-e^+e^-$ invariant mass, (top right) $\cos\theta_\ell$, (bottom left) $\cos\theta_K$ and (bottom right) $\tilde{\phi}$ variables of $B^0 \rightarrow K^{*0}e^+e^-$ candidates in the reconstructed q^2 range between 10^{-4} GeV^2 and 0.25 GeV^2 . The black points represent the data, while the solid blue curve shows the total PDF. The signal component is represented by the dashed red line and the shaded areas are the background components, as detailed in the legend. The SL/C component is composed of semileptonic and combinatorial background contributions. The dashed vertical lines indicate the restricted mass range used in the angular analysis.

shape, which depends only on the parameter F_L . The value of F_L for the $B^0 \rightarrow K^{*0}\gamma$ decay is obtained from the fit to the control sample detailed in Sec. 8. When included as a background in the fit to the signal sample, the $B^0 \rightarrow K^{*0}\gamma$ angular shape is obtained from the simulation sample and is assumed to factorise between the angles.

The background contributions due to $B^0 \rightarrow K^{*0}\eta$ and $B^0 \rightarrow K^{*0}\pi^0$ decays that contribute to the signal and control samples are modelled using simulation and are also assumed to factorise in the three angles. Since this background has $F_L = 1$ due to the π^0 or η angular momentum, the $\cos\theta_K$ distribution has a very different shape compared to $B^0 \rightarrow K^{*0}e^+e^-$ decays. Its precise modelling is validated by the measurement of the F_L parameter in the control channel reported in Sec. 8.

The angular shape of the PR background is modelled using the same functional shape as the signal, determined from $B^+ \rightarrow K_1(1270)e^+e^-$ simulated events, where one of the pions from the $K_1(1270) \rightarrow K^+\pi^-\pi^+$ decay is not reconstructed.

A sample of $B^0 \rightarrow K^{*0}e^+\mu^-$ candidates from LHCb data is used to determine the SL/C angular shapes. Since this decay is forbidden in the SM due to lepton flavour conservation, this sample will mostly comprise semileptonic and combinatorial background events. The q^2 and BDT requirements are slightly relaxed to increase the sample size. It is checked that this sample is a good proxy for SL/C background by assigning the muon candidate an electron mass and comparing the resulting angular and $K^+\pi^-e^+e^-$ invariant-mass distributions to those of $B^0 \rightarrow K^{*0}e^+e^-$ decays in the upper mass sideband and low BDT output regions. The angular shapes of the three angles are found to factorise in this sample and therefore are modelled separately.

8 Angular observables

To determine the four angular observables, F_L , $A_T^{(2)}$, A_T^{Im} and A_T^{Re} , an unbinned maximum likelihood fit is performed to the $m(K^+\pi^-e^+e^-)$, $\cos\theta_\ell$, $\cos\theta_K$ and $\tilde{\phi}$ distributions in a restricted $m(K^+\pi^-e^+e^-)$ window between 5000 and 5400 MeV. The inclusion of $m(K^+\pi^-e^+e^-)$ improves the statistical power of the fit since, even within the restricted window, the mass shapes of the signal and of the background contributions are very different. The fractions of the fit components are constrained using a multivariate Gaussian function to the results in the wide mass range extrapolated to the narrow mass range. Pseudoexperiments are used to assess the impact of fitting the $m(K^+\pi^-e^+e^-)$ distribution again in the restricted range. The resulting bias is found to be negligible.

The fitting procedure is verified using a large sample of fully simulated events, with the obtained values of F_L , $A_T^{(2)}$, A_T^{Im} and A_T^{Re} in excellent agreement with the inputs. The $B^0 \rightarrow K^{*0}e^+e^-$ fit is then validated on data by performing a similar fit to the $m(K^+\pi^-e^+e^-)$ and $\cos\theta_K$ distributions of the control sample. The $\cos\theta_K$ distribution for the control sample, together with the PDF projections resulting from the fit, are shown in Fig. 2. The fitted value of $F_L = 0.0_{-0.0}^{+0.7}\%$ is compatible with a completely transverse K^{*0} polarisation, as expected due to presence of the real photon. Finally, the $B^0 \rightarrow K^{*0}e^+e^-$ fit is further validated using 10 000 pseudoexperiments including signal and background components. Several input values for the angular observables, F_L , $A_T^{(2)}$, A_T^{Im} and A_T^{Re} , are studied including those associated with BSM models, and the results are in good agreement with the inputs, with the exception of F_L , where a small bias at the level of 7% of its statistical uncertainty is observed and corrected for. Furthermore, the non-negligible

size of the $\tilde{\phi}$ resolution results in an underestimation of the magnitude of $A_T^{(2)}$ and A_T^{Im} by 4%. Although this shift is negligibly small for the magnitudes expected in the SM, it could be sizeable for large C_7' values and therefore the $A_T^{(2)}$ and A_T^{Im} values are corrected for this effect. The angular distributions, $\cos\theta_\ell$, $\cos\theta_K$ and $\tilde{\phi}$, for the signal region, together with the PDF projections resulting from the fit, are shown in Fig. 3. Results for the angular observables are given in Sec. 10.

9 Systematic uncertainties

To evaluate systematic uncertainties resulting from the limited size of the data and simulation samples used to determine the angular shapes and acceptances, a bootstrapping technique is used [63]. In addition, systematic uncertainties related to various modelling choices used in the fits are evaluated by generating pseudoexperiments with an alternative model and fitting with the nominal model used to fit the data. The results of the mass and angular fits are then compared with the input values to assess the size of the uncertainties. The alternative modelling choices considered are detailed in the following.

The systematic uncertainties related to the corrections applied to simulated events used to model the angular acceptance are evaluated by fitting uncorrected simulated events. An alternative model using Legendre polynomials of order six instead of four is used to estimate the systematic uncertainties related to the shape of the acceptance function.

To take into account possible variations in the angular shapes of the PR background due to states other than the $K_1(1270)$ meson, alternative shapes are determined from a sample of $B^+ \rightarrow K^+\pi^-\pi^+e^+e^-$ simulated events. This sample is reweighted in the $K^+\pi^-\pi^+$ Dalitz plane to match the distribution in $B^+ \rightarrow J/\psi(\rightarrow e^+e^-)K^{\text{res}}(\rightarrow K^+\pi^-\pi^+)$ data, where K^{res} is any kaon resonance that decays to $K^+\pi^-\pi^+$. Alternative models for the SL/C background are obtained by tightening either the q^2 or BDT requirements used

Table 1: Summary of systematic uncertainties on the four angular observables, $A_T^{(2)}$, A_T^{Im} , A_T^{Re} and F_L . The total systematic uncertainty is the sum in quadrature of all the contributions. For comparison, the statistical uncertainties are shown in the last row of the table.

Source of systematic	$A_T^{(2)}$	A_T^{Im}	A_T^{Re}	F_L
Simulation sample size for acceptance	0.007	0.007	0.007	0.003
Acceptance function modelling	0.004	0.001	0.008	0.001
$B^0 \rightarrow K^{*0}e^+\mu^-$ sample size for SL/C	0.007	0.007	0.007	0.003
SL/C angular modelling	0.012	0.005	0.006	0.005
PR model other than $K_1(1270)$	0.001	0.003	0.002	0.001
η or π^0 angular modelling	< 0.001	< 0.001	0.002	0.010
Corrections to simulation	0.003	0.001	0.003	0.007
Signal mass shape	0.002	0.002	0.004	0.001
Total systematic uncertainty	0.017	0.012	0.015	0.014
Statistical uncertainty	0.103	0.102	0.077	0.026

in the $B^0 \rightarrow K^{*0}e^+\mu^-$ selection.

To estimate the systematic uncertainty due to differences between data and simulation in the $B^0 \rightarrow K^{*0}e^+e^-$ mass shapes, the signal mass PDF is corrected using a fit to the $B^0 \rightarrow K^{*0}\gamma$ rather than the $B^0 \rightarrow J/\psi(e^+e^-)K^{*0}$ channel. The systematic uncertainties are summarised in Table 1. The total systematic uncertainty, obtained by adding all individual sources in quadrature, is smaller than the statistical uncertainty for all observables.

10 Results

The four $B^0 \rightarrow K^{*0}e^+e^-$ angular observables measured in the effective q^2 range from 0.0008 to 0.257 GeV² are found to be

$$\begin{aligned} F_L &= 0.044 \pm 0.026 \pm 0.014, \\ A_T^{\text{Re}} &= -0.06 \pm 0.08 \pm 0.02, \\ A_T^{(2)} &= +0.11 \pm 0.10 \pm 0.02, \\ A_T^{\text{Im}} &= +0.02 \pm 0.10 \pm 0.01, \end{aligned}$$

where the first contribution to the uncertainty is statistical and the second systematic. Correlations between the observables are measured to be

	F_L	A_T^{Re}	$A_T^{(2)}$	A_T^{Im}
F_L	1.00	-0.02	-0.01	0.02
A_T^{Re}		1.00	0.05	0.02
$A_T^{(2)}$			1.00	0.10
A_T^{Im}				1.00

These results supersede Ref. [21]. Using Eq. 2, the measured $A_T^{(2)}$ and A_T^{Im} observables are used to determine the photon polarisation in $B^0 \rightarrow K^{*0}\gamma$ decays

$$\begin{aligned} \text{Re}(A_R/A_L) &= 0.05 \pm 0.05 \\ \text{Im}(A_R/A_L) &= 0.01 \pm 0.05. \end{aligned}$$

Furthermore, using the FLAVIO software package [46], these measurements can be used to determine the polarisation of the $b \rightarrow s\gamma$ transition, which can be expressed as the ratio of the right- and left-handed $C_7^{(\prime)}$ Wilson coefficients. Details about the calculations of hadronic contributions can be found in Ref. [10]. The obtained constraints are shown in Fig. 4, where they are compared to those from previous measurements by the Belle, BaBar and LHCb experiments [11–18]. Here, the $C_7^{(\prime)}$ regularisation-scheme independent effective coefficients are calculated at the scale $\mu = 4.8$ GeV [10]. The value of the left-handed C_7 coefficient is fixed to its SM value, $C_7^{\text{SM}} = -0.2915$. Theoretical uncertainties related to the predictions of the experimental observables are taken into account in the constrained areas. The results presented in this paper provide the world’s best constraint on the $b \rightarrow s\gamma$ photon polarisation.

11 Conclusion

An angular analysis of the $B^0 \rightarrow K^{*0}e^+e^-$ decay is performed using proton-proton collision data, corresponding to an integrated luminosity of 9.0 fb⁻¹, collected by the

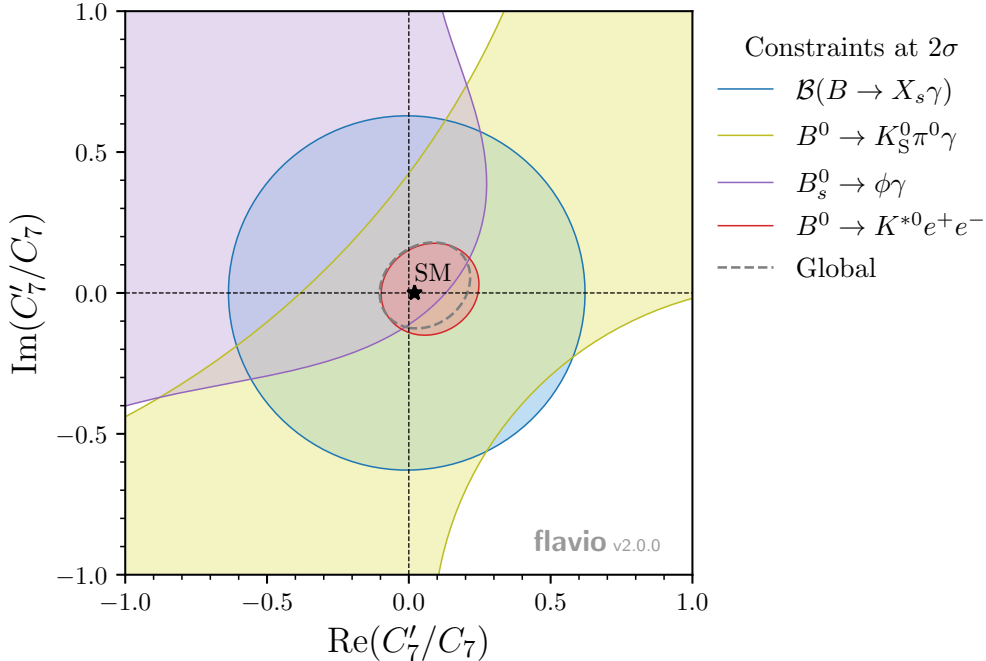


Figure 4: Constraints at 2σ level on the real and imaginary parts of the ratio of right- and left-handed Wilson coefficients, C'_7 and C_7 . The C_7 coefficient is fixed to its SM value. The measurements of the inclusive branching fraction, $\mathcal{B}(B \rightarrow X_s \gamma)$, and the $B^0 \rightarrow K_S^0 \pi^0 \gamma$ mixing-induced CP asymmetry by the Belle and BaBar experiments [11–17] are shown in blue and yellow, respectively, the $B_s^0 \rightarrow \phi \gamma$ measurements at LHCb [18] in purple and the measurement presented in this paper in red. The global fit is shown in dashed lines and the SM prediction is represented by a black star and corresponds to the ratio of s - and b -quark masses.

LHCb experiment between 2011 and 2018. Angular observables are measured for the first time in the q^2 range from 0.0008 to 0.257 GeV².

The results are consistent with SM predictions [24, 43, 46] and are used to measure both the real and imaginary parts of the $B^0 \rightarrow K^{*0} \gamma$ photon polarisation with a precision of 5%. Furthermore, the results of this paper make it possible to constrain the $b \rightarrow s \gamma$ photon polarisation with significantly better precision than the combination of previous measurements.

Acknowledgements

We express our gratitude to our colleagues in the CERN accelerator departments for the excellent performance of the LHC. We thank the technical and administrative staff at the LHCb institutes. We acknowledge support from CERN and from the national agencies: CAPES, CNPq, FAPERJ and FINEP (Brazil); MOST and NSFC (China); CNRS/IN2P3 (France); BMBF, DFG and MPG (Germany); INFN (Italy); NWO (Netherlands); MNiSW and NCN (Poland); MEN/IFA (Romania); MSHE (Russia); MICINN (Spain); SNSF and SER (Switzerland); NASU (Ukraine); STFC (United Kingdom); DOE NP and NSF (USA). We acknowledge the computing resources that are provided by CERN, IN2P3 (France), KIT and DESY (Germany), INFN (Italy), SURF (Netherlands), PIC (Spain),

GridPP (United Kingdom), RRCKI and Yandex LLC (Russia), CSCS (Switzerland), IFIN-HH (Romania), CBPF (Brazil), PL-GRID (Poland) and OSC (USA). We are indebted to the communities behind the multiple open-source software packages on which we depend. Individual groups or members have received support from AvH Foundation (Germany); EPLANET, Marie Skłodowska-Curie Actions and ERC (European Union); A*MIDEX, ANR, Labex P2IO and OCEVU, and Région Auvergne-Rhône-Alpes (France); Key Research Program of Frontier Sciences of CAS, CAS PIFI, Thousand Talents Program, and Sci. & Tech. Program of Guangzhou (China); RFBR, RSF and Yandex LLC (Russia); GVA, XuntaGal and GENCAT (Spain); the Royal Society and the Leverhulme Trust (United Kingdom).

References

- [1] D. Atwood, M. Gronau, and A. Soni, *Mixing induced CP asymmetries in radiative B decays in and beyond the standard model*, Phys. Rev. Lett. **79** (1997) 185, [arXiv:hep-ph/9704272](#).
- [2] L. L. Everett *et al.*, *Alternative approach to $b \rightarrow s\gamma$ in the $uMSSM$* , JHEP **01** (2002) 022, [arXiv:hep-ph/0112126](#).
- [3] B. Grinstein, Y. Grossman, Z. Ligeti, and D. Pirjol, *The Photon polarization in $B \rightarrow X\gamma$ in the standard model*, Phys. Rev. **D71** (2005) 011504, [arXiv:hep-ph/0412019](#).
- [4] J. Foster, K.-i. Okumura, and L. Roszkowski, *New constraints on SUSY flavour mixing in light of recent measurements at the Tevatron*, Phys. Lett. **B641** (2006) 452, [arXiv:hep-ph/0604121](#).
- [5] E. Lunghi and J. Matias, *Huge right-handed current effects in $B \rightarrow K^{*0}(K\pi)\ell^+\ell^-$ in supersymmetry*, JHEP **04** (2007) 058, [arXiv:hep-ph/0612166](#).
- [6] T. Goto, Y. Okada, T. Shindou, and M. Tanaka, *Patterns of flavor signals in supersymmetric models*, Phys. Rev. **D77** (2008) 095010, [arXiv:0711.2935](#).
- [7] D. Bećirević, E. Kou, A. Le Yaouanc, and A. Tayduganov, *Future prospects for the determination of the Wilson coefficient $C'_{7\gamma}$* , JHEP **08** (2012) 090, [arXiv:1206.1502](#).
- [8] E. Kou, C.-D. Lü, and F.-S. Yu, *Photon polarization in the $b \rightarrow s\gamma$ processes in the Left-Right Symmetric Model*, JHEP **12** (2013) 102, [arXiv:1305.3173](#).
- [9] N. Haba *et al.*, *Search for new physics via photon polarization of $b \rightarrow s\gamma$* , JHEP **03** (2015) 160, [arXiv:1501.00668](#).
- [10] A. Paul and D. M. Straub, *Constraints on new physics from radiative B decays*, JHEP **04** (2017) 027, [arXiv:1608.02556](#).
- [11] BaBar collaboration, B. Aubert *et al.*, *Measurement of the $B \rightarrow X_s\gamma$ branching fraction and photon energy spectrum using the recoil method*, Phys. Rev. **D77** (2008) 051103, [arXiv:0711.4889](#).

- [12] BaBar collaboration, J. P. Lees *et al.*, *Precision measurement of the $B \rightarrow X_s \gamma$ photon energy spectrum, branching fraction, and direct CP asymmetry $A_{CP}(B \rightarrow X_{s+d} \gamma)$* , Phys. Rev. Lett. **109** (2012) 191801, [arXiv:1207.2690](#).
- [13] BaBar collaboration, J. P. Lees *et al.*, *Exclusive Measurements of $b \rightarrow s \gamma$ Transition Rate and Photon Energy Spectrum*, Phys. Rev. **D86** (2012) 052012, [arXiv:1207.2520](#).
- [14] Belle collaboration, T. Saito *et al.*, *Measurement of the $\bar{B} \rightarrow X_s \gamma$ branching fraction with a sum of exclusive decays*, Phys. Rev. **D91** (2015) 052004, [arXiv:1411.7198](#).
- [15] Belle collaboration, A. Abdesselam *et al.*, *Measurement of the inclusive $B \rightarrow X_{s+d} \gamma$ branching fraction, photon energy spectrum and HQE parameters*, in *38th International Conference on High Energy Physics*, 2016, [arXiv:1608.02344](#).
- [16] Belle collaboration, Y. Ushiroda *et al.*, *Time-dependent CP asymmetries in $B^0 \rightarrow K_S^0 \pi^0 \gamma$ transitions*, Phys. Rev. **D74** (2006) 111104, [arXiv:hep-ex/0608017](#).
- [17] BaBar collaboration, B. Aubert *et al.*, *Measurement of Time-Dependent CP Asymmetry in $B^0 \rightarrow K_S^0 \pi^0 \gamma$ Decays*, Phys. Rev. **D78** (2008) 071102, [arXiv:0807.3103](#).
- [18] LHCb collaboration, R. Aaij *et al.*, *Measurement of CP-violating and mixing-induced observables in $B_s^0 \rightarrow \phi \gamma$ decays*, Phys. Rev. Lett. **123** (2019) 081802, [arXiv:1905.06284](#).
- [19] Y. Grossman and D. Pirjol, *Extracting and using photon polarization information in radiative B decays*, JHEP **06** (2000) 029, [arXiv:hep-ph/0005069](#).
- [20] S. Jäger and J. M. Camalich, *On $B \rightarrow V \ell \ell$ at small dilepton invariant mass, power corrections, and new physics*, JHEP **05** (2013) 043, [arXiv:1212.2263](#).
- [21] LHCb collaboration, R. Aaij *et al.*, *Angular analysis of the $B^0 \rightarrow K^* e^+ e^-$ decay in the low- q^2 region*, JHEP **04** (2015) 064, [arXiv:1501.03038](#).
- [22] A. Bharucha, D. M. Straub, and R. Zwicky, *$B \rightarrow V \ell^+ \ell^-$ in the Standard Model from light-cone sum rules*, JHEP **08** (2016) 098, [arXiv:1503.05534](#).
- [23] P. Ball, G. W. Jones, and R. Zwicky, *$B \rightarrow V \gamma$ beyond QCD factorisation*, Phys. Rev. **D75** (2007) 054004, [arXiv:hep-ph/0612081](#).
- [24] S. Jäger and J. Martin Camalich, *Reassessing the discovery potential of the $B \rightarrow K^* \ell^+ \ell^-$ decays in the large-recoil region: SM challenges and BSM opportunities*, Phys. Rev. D **93** (2016) 014028, [arXiv:1412.3183](#).
- [25] J. Lyon and R. Zwicky, *Resonances gone topsy turvy - the charm of QCD or new physics in $b \rightarrow s \ell^+ \ell^-$?*, [arXiv:1406.0566](#).
- [26] M. Ciuchini *et al.*, *$B \rightarrow K^* \ell^+ \ell^-$ decays at large recoil in the Standard Model: a theoretical reappraisal*, JHEP **06** (2016) 116, [arXiv:1512.07157](#).
- [27] C. Bobeth, M. Chrzaszcz, D. van Dyk, and J. Virto, *Long-distance effects in $B \rightarrow K^* \ell \ell$ from analyticity*, Eur. Phys. J. **C78** (2018) 451, [arXiv:1707.07305](#).

- [28] LHCb collaboration, R. Aaij *et al.*, *Measurement of CP-averaged observables in the $B^0 \rightarrow K^{*0}\mu^+\mu^-$ decay*, Phys. Rev. Lett. **125** (2020) 011802, arXiv:2003.04831.
- [29] LHCb collaboration, R. Aaij *et al.*, *Differential branching fractions and isospin asymmetries of $B \rightarrow K^{(*)}\mu^+\mu^-$ decays*, JHEP **06** (2014) 133, arXiv:1403.8044.
- [30] LHCb collaboration, R. Aaij *et al.*, *Angular analysis and differential branching fraction of the decay $B_s^0 \rightarrow \phi\mu^+\mu^-$* , JHEP **09** (2015) 179, arXiv:1506.08777.
- [31] LHCb collaboration, R. Aaij *et al.*, *Differential branching fraction and angular analysis of $\Lambda_b^0 \rightarrow \Lambda\mu^+\mu^-$ decays*, JHEP **06** (2015) 115, Erratum *ibid.* **09** (2018) 145, arXiv:1503.07138.
- [32] LHCb collaboration, R. Aaij *et al.*, *Search for lepton-universality violation in $B^+ \rightarrow K^+\ell^+\ell^-$ decays*, Phys. Rev. Lett. **122** (2019) 191801, arXiv:1903.09252.
- [33] LHCb collaboration, R. Aaij *et al.*, *Test of lepton universality with $B^0 \rightarrow K^{*0}\ell^+\ell^-$ decays*, JHEP **08** (2017) 055, arXiv:1705.05802.
- [34] M. Algueró *et al.*, *Emerging patterns of New Physics with and without Lepton Flavour Universal contributions*, Eur. Phys. J. **C79** (2019) 714, Addendum *ibid.* **C80** (2020) 511, arXiv:1903.09578.
- [35] J. Aebischer *et al.*, *B-decay discrepancies after Moriond 2019*, Eur. Phys. J. **C80** (2020) 252, arXiv:1903.10434.
- [36] A. Crivellin, C. Greub, D. Müller, and F. Saturnino, *Importance of loop effects in explaining the accumulated evidence for New Physics in B decays with a vector leptoquark*, Phys. Rev. Lett. **122** (2019) 011805, arXiv:1807.02068.
- [37] A. Arbey *et al.*, *Update on the $b \rightarrow s$ anomalies*, Phys. Rev. **D100** (2019) 015045, arXiv:1904.08399.
- [38] M. Ciuchini *et al.*, *New Physics in $b \rightarrow s\ell^+\ell^-$ confronts new data on lepton universality*, Eur. Phys. J. **C79** (2019) 719, arXiv:1903.09632.
- [39] LHCb collaboration, R. Aaij *et al.*, *Differential branching fraction and angular analysis of the decay $B^0 \rightarrow K^{*0}\mu^+\mu^-$* , JHEP **08** (2013) 131, arXiv:1304.6325.
- [40] LHCb collaboration, R. Aaij *et al.*, *Measurements of the S-wave fraction in $B^0 \rightarrow K^+\pi^-\mu^+\mu^-$ decays and the $B^0 \rightarrow K^*(892)^0\mu^+\mu^-$ differential branching fraction*, JHEP **11** (2016) 047, Erratum *ibid.* **04** (2017) 142, arXiv:1606.04731.
- [41] F. Krüger and J. Matias, *Probing new physics via the transverse amplitudes of $B^0 \rightarrow K^{*0}(\rightarrow K^-\pi^+)\ell^+\ell^-$ at large recoil*, Phys. Rev. **D71** (2005) 094009, arXiv:hep-ph/0502060.
- [42] C.-D. Lü and W. Wang, *Analysis of $B \rightarrow K_j^*(\rightarrow K\pi)\mu^+\mu^-$ in the higher kaon resonance region*, Phys. Rev. **D85** (2012) 034014, arXiv:1111.1513.
- [43] D. Bećirević and E. Schneider, *On transverse asymmetries in $B \rightarrow K^*\ell^+\ell^-$* , Nucl. Phys. **B854** (2012) 321, arXiv:1106.3283.

- [44] C. Bobeth, G. Hiller, and G. Piranishvili, *CP asymmetries in $\bar{B} \rightarrow \bar{K}^*(\rightarrow \bar{K}\pi)\bar{\ell}\ell$ and untagged $\bar{B}_s, B_s \rightarrow \phi(\rightarrow K^+K^-)\bar{\ell}\ell$ decays at NLO*, JHEP **07** (2008) 106, arXiv:0805.2525.
- [45] S. Descotes-Genon, J. Matias, M. Ramon, and J. Virto, *Implications from clean observables for the binned analysis of $B \rightarrow K^*\mu^+\mu^-$ at large recoil*, JHEP **01** (2013) 048, arXiv:1207.2753.
- [46] D. M. Straub, *flavio: a Python package for flavour and precision phenomenology in the Standard Model and beyond*, arXiv:1810.08132.
- [47] LHCb collaboration, A. A. Alves Jr. *et al.*, *The LHCb detector at the LHC*, JINST **3** (2008) S08005.
- [48] LHCb collaboration, R. Aaij *et al.*, *LHCb detector performance*, Int. J. Mod. Phys. **A30** (2015) 1530022, arXiv:1412.6352.
- [49] V. V. Gligorov and M. Williams, *Efficient, reliable and fast high-level triggering using a bonsai boosted decision tree*, JINST **8** (2013) P02013, arXiv:1210.6861.
- [50] T. Sjöstrand, S. Mrenna, and P. Skands, *PYTHIA 6.4 physics and manual*, JHEP **05** (2006) 026, arXiv:hep-ph/0603175; T. Sjöstrand, S. Mrenna, and P. Skands, *A brief introduction to PYTHIA 8.1*, Comput. Phys. Commun. **178** (2008) 852, arXiv:0710.3820.
- [51] I. Belyaev *et al.*, *Handling of the generation of primary events in Gauss, the LHCb simulation framework*, J. Phys. Conf. Ser. **331** (2011) 032047.
- [52] D. J. Lange, *The EvtGen particle decay simulation package*, Nucl. Instrum. Meth. **A462** (2001) 152.
- [53] P. Golonka and Z. Was, *PHOTOS Monte Carlo: A precision tool for QED corrections in Z and W decays*, Eur. Phys. J. **C45** (2006) 97, arXiv:hep-ph/0506026.
- [54] Geant4 collaboration, J. Allison *et al.*, *Geant4 developments and applications*, IEEE Trans. Nucl. Sci. **53** (2006) 270; Geant4 collaboration, S. Agostinelli *et al.*, *Geant4: A simulation toolkit*, Nucl. Instrum. Meth. **A506** (2003) 250.
- [55] M. Clemencic *et al.*, *The LHCb simulation application, Gauss: Design, evolution and experience*, J. Phys. Conf. Ser. **331** (2011) 032023.
- [56] Particle Data Group, P. A. Zyla *et al.*, *Review of particle physics*, Prog. Theor. Exp. Phys. **2020** (2020) 083C01.
- [57] M. Alexander *et al.*, *Mapping the material in the LHCb vertex locator using secondary hadronic interactions*, JINST **13** (2018) P06008, arXiv:1803.07466.
- [58] Y.-S. Tsai, *Pair Production and Bremsstrahlung of Charged Leptons*, Rev. Mod. Phys. **46** (1974) 815, Erratum *ibid.* **49** (1977) 521.
- [59] L. Breiman, J. H. Friedman, R. A. Olshen, and C. J. Stone, *Classification and regression trees*, Wadsworth international group, Belmont, California, USA, 1984.

- [60] Y. Freund and R. E. Schapire, *A decision-theoretic generalization of on-line learning and an application to boosting*, J. Comput. Syst. Sci. **55** (1997) 119.
- [61] T. Skwarnicki, *A study of the radiative cascade transitions between the Upsilon-prime and Upsilon resonances*, PhD thesis, Institute of Nuclear Physics, Krakow, 1986, DESY-F31-86-02.
- [62] K. S. Cranmer, *Kernel estimation in high-energy physics*, Comput. Phys. Commun. **136** (2001) 198, [arXiv:hep-ex/0011057](https://arxiv.org/abs/hep-ex/0011057).
- [63] B. Efron, *Bootstrap methods: Another look at the jackknife*, Ann. Statist. **7** (1979) 1.

LHCb collaboration

R. Aaij³¹, C. Abellán Beteta⁴⁹, T. Ackernley⁵⁹, B. Adeva⁴⁵, M. Adinolfi⁵³, H. Afsharnia⁹, C.A. Aidala⁸⁴, S. Aiola²⁵, Z. Ajaltouni⁹, S. Akar⁶⁴, J. Albrecht¹⁴, F. Alessio⁴⁷, M. Alexander⁵⁸, A. Alfonso Alberio⁴⁴, Z. Aliouche⁶¹, G. Alkhazov³⁷, P. Alvarez Cartelle⁴⁷, S. Amato², Y. Amhis¹¹, L. An²¹, L. Anderlini²¹, A. Andreianov³⁷, M. Andreotti²⁰, F. Archilli¹⁶, A. Artamonov⁴³, M. Artuso⁶⁷, K. Arzymatov⁴¹, E. Aslanides¹⁰, M. Atzeni⁴⁹, B. Audurier¹¹, S. Bachmann¹⁶, M. Bachmayer⁴⁸, J.J. Back⁵⁵, S. Baker⁶⁰, P. Baladron Rodriguez⁴⁵, V. Balagura¹¹, W. Baldini²⁰, J. Baptista Leite¹, R.J. Barlow⁶¹, S. Barsuk¹¹, W. Barter⁶⁰, M. Bartolini^{23,i}, F. Baryshnikov⁸⁰, J.M. Basels¹³, G. Bassi²⁸, B. Batsukh⁶⁷, A. Battig¹⁴, A. Bay⁴⁸, M. Becker¹⁴, F. Bedeschi²⁸, I. Bediaga¹, A. Beiter⁶⁷, V. Belavin⁴¹, S. Belin²⁶, V. Bellee⁴⁸, K. Belous⁴³, I. Belov³⁹, I. Belyaev³⁸, G. Bencivenni²², E. Ben-Haim¹², A. Berezhnoy³⁹, R. Bernet⁴⁹, D. Berninghoff¹⁶, H.C. Bernstein⁶⁷, C. Bertella⁴⁷, E. Bertholet¹², A. Bertolin²⁷, C. Betancourt⁴⁹, F. Betti^{19,e}, M.O. Bettler⁵⁴, Ia. Bezshyiko⁴⁹, S. Bhasin⁵³, J. Bhom³³, L. Bian⁷², M.S. Bieker¹⁴, S. Bifani⁵², P. Billoir¹², M. Birch⁶⁰, F.C.R. Bishop⁵⁴, A. Bizzeti^{21,s}, M. Bjørn⁶², M.P. Blago⁴⁷, T. Blake⁵⁵, F. Blanc⁴⁸, S. Blusk⁶⁷, D. Bobulska⁵⁸, V. Bocci³⁰, J.A. Boelhauve¹⁴, O. Boente Garcia⁴⁵, T. Boettcher⁶³, A. Boldyrev⁸¹, A. Bondar^{42,v}, N. Bondar³⁷, S. Borghi⁶¹, M. Borisyak⁴¹, M. Borsato¹⁶, J.T. Borsuk³³, S.A. Bouchiba⁴⁸, T.J.V. Bowcock⁵⁹, A. Boyer⁴⁷, C. Bozzi²⁰, M.J. Bradley⁶⁰, J.T. Brandt¹⁶, S. Braun⁶⁵, A. Brea Rodriguez⁴⁵, M. Brodski⁴⁷, J. Brodzicka³³, A. Brossa Gonzalo⁵⁵, D. Brundu²⁶, A. Buonaura⁴⁹, C. Burr⁴⁷, A. Bursche²⁶, A. Butkevich⁴⁰, J.S. Butter³¹, J. Buytaert⁴⁷, W. Byczynski⁴⁷, S. Cadeddu²⁶, H. Cai⁷², R. Calabrese^{20,g}, L. Calefice¹⁴, L. Calero Diaz²², S. Cali²², R. Calladine⁵², M. Calvi^{24,j}, M. Calvo Gomez⁸³, P. Camargo Magalhaes⁵³, A. Camboni⁴⁴, P. Campana²², D.H. Campora Perez⁴⁷, A.F. Campoverde Quezada⁵, S. Capelli^{24,j}, L. Capriotti^{19,e}, A. Carbone^{19,e}, G. Carboni²⁹, R. Cardinale^{23,i}, A. Cardini²⁶, I. Carli⁶, P. Carniti^{24,j}, K. Carvalho Akiba³¹, A. Casais Vidal⁴⁵, G. Casse⁵⁹, M. Cattaneo⁴⁷, G. Cavallero⁴⁷, S. Celani⁴⁸, J. Cerasoli¹⁰, A.J. Chadwick⁵⁹, M.G. Chapman⁵³, M. Charles¹², Ph. Charpentier⁴⁷, G. Chatzikonstantinidis⁵², C.A. Chavez Barajas⁵⁹, M. Chefdeville⁸, C. Chen³, S. Chen²⁶, A. Chernov³³, S.-G. Chitic⁴⁷, V. Chobanova⁴⁵, S. Cholak⁴⁸, M. Chruszcz³³, A. Chubykin³⁷, V. Chulikov³⁷, P. Ciambone²², M.F. Cicala⁵⁵, X. Cid Vidal⁴⁵, G. Ciezarek⁴⁷, P.E.L. Clarke⁵⁷, M. Clemencic⁴⁷, H.V. Cliff⁵⁴, J. Closier⁴⁷, J.L. Cobbedick⁶¹, V. Coco⁴⁷, J.A.B. Coelho¹¹, J. Cogan¹⁰, E. Cogneras⁹, L. Cojocariu³⁶, P. Collins⁴⁷, T. Colombo⁴⁷, L. Congedo¹⁸, A. Contu²⁶, N. Cooke⁵², G. Coombs⁵⁸, G. Corti⁴⁷, C.M. Costa Sobral⁵⁵, B. Couturier⁴⁷, D.C. Craik⁶³, J. Crkovská⁶⁶, M. Cruz Torres¹, R. Currie⁵⁷, C.L. Da Silva⁶⁶, E. Dall'Occo¹⁴, J. Dalseno⁴⁵, C. D'Ambrosio⁴⁷, A. Danilina³⁸, P. d'Argent⁴⁷, A. Davis⁶¹, O. De Aguiar Francisco⁶¹, K. De Bruyn⁷⁷, S. De Capua⁶¹, M. De Cian⁴⁸, J.M. De Miranda¹, L. De Paula², M. De Serio^{18,d}, D. De Simone⁴⁹, P. De Simone²², J.A. de Vries⁷⁸, C.T. Dean⁶⁶, W. Dean⁸⁴, D. Decamp⁸, L. Del Buono¹², B. Delaney⁵⁴, H.-P. Dembinski¹⁴, A. Dendek³⁴, V. Denysenko⁴⁹, D. Derkach⁸¹, O. Deschamps⁹, F. Desse¹¹, F. Dettori^{26,f}, B. Dey⁷², P. Di Nezza²², S. Didenko⁸⁰, L. Dieste Maronas⁴⁵, H. Dijkstra⁴⁷, V. Dobishuk⁵¹, A.M. Donohoe¹⁷, F. Dordei²⁶, M. Dorigo^{28,w}, A.C. dos Reis¹, L. Douglas⁵⁸, A. Dovbnya⁵⁰, A.G. Downes⁸, K. Dreimanis⁵⁹, M.W. Dudek³³, L. Dufour⁴⁷, V. Duk⁷⁶, P. Durante⁴⁷, J.M. Durham⁶⁶, D. Dutta⁶¹, M. Dziurda¹⁶, A. Dziurda³³, A. Dzyuba³⁷, S. Easo⁵⁶, U. Egede⁶⁸, V. Egorychev³⁸, S. Eidelman^{42,v}, S. Eisenhardt⁵⁷, S. Ek-In⁴⁸, L. Eklund⁵⁸, S. Ely⁶⁷, A. Ene³⁶, E. Eppe⁶⁶, S. Escher¹³, J. Eschle⁴⁹, S. Esen³¹, T. Evans⁴⁷, A. Falabella¹⁹, J. Fan³, Y. Fan⁵, B. Fang⁷², N. Farley⁵², S. Farry⁵⁹, D. Fazzini^{24,j}, P. Fedin³⁸, M. Féo⁴⁷, P. Fernandez Declara⁴⁷, A. Fernandez Prieto⁴⁵, J.M. Fernandez-tenllado Arribas⁴⁴, F. Ferrari^{19,e}, L. Ferreira Lopes⁴⁸, F. Ferreira Rodrigues², S. Ferreres Sole³¹, M. Ferrillo⁴⁹, M. Ferro-Luzzi⁴⁷, S. Filippov⁴⁰, R.A. Fini¹⁸, M. Fiorini^{20,g}, M. Firlej³⁴, K.M. Fischer⁶², C. Fitzpatrick⁶¹, T. Fiutowski³⁴, F. Fleuret^{11,b}, M. Fontana⁴⁷, F. Fontanelli^{23,i}, R. Forty⁴⁷,

V. Franco Lima⁵⁹, M. Franco Sevilla⁶⁵, M. Frank⁴⁷, E. Franzoso²⁰, G. Frau¹⁶, C. Frei⁴⁷,
 D.A. Friday⁵⁸, J. Fu²⁵, Q. Fuehring¹⁴, W. Funk⁴⁷, E. Gabriel³¹, T. Gaintseva⁴¹,
 A. Gallas Torreira⁴⁵, D. Galli^{19,e}, S. Gallorini²⁷, S. Gambetta⁵⁷, Y. Gan³, M. Gandelman²,
 P. Gandini²⁵, Y. Gao⁴, M. Garau²⁶, L.M. Garcia Martin⁵⁵, P. Garcia Moreno⁴⁴,
 J. García Pardiñas⁴⁹, B. Garcia Plana⁴⁵, F.A. Garcia Rosales¹¹, L. Garrido⁴⁴, D. Gascon⁴⁴,
 C. Gaspar⁴⁷, R.E. Geertsema³¹, D. Gerick¹⁶, L.L. Gerken¹⁴, E. Gersabeck⁶¹, M. Gersabeck⁶¹,
 T. Gershon⁵⁵, D. Gerstel¹⁰, Ph. Ghez⁸, V. Gibson⁵⁴, M. Giovannetti^{22,k}, A. Gioventù⁴⁵,
 P. Gironella Gironell⁴⁴, L. Giubega³⁶, C. Giugliano^{20,g}, K. Gizdov⁵⁷, E.L. Gkougkousis⁴⁷,
 V.V. Gligorov¹², C. Göbel⁶⁹, E. Golobardes⁸³, D. Golubkov³⁸, A. Golutvin^{60,80}, A. Gomes^{1,a},
 S. Gomez Fernandez⁴⁴, F. Goncalves Abrantes⁶⁹, M. Goncerz³³, G. Gong³, P. Gorbounov³⁸,
 I.V. Gorelov³⁹, C. Gotti^{24,j}, E. Govorkova³¹, J.P. Grabowski¹⁶, R. Graciani Diaz⁴⁴,
 T. Grammatico¹², L.A. Granado Cardoso⁴⁷, E. Graugés⁴⁴, E. Graverini⁴⁸, G. Graziani²¹,
 A. Grecu³⁶, L.M. Greeven³¹, P. Griffith²⁰, L. Grillo⁶¹, S. Gromov⁸⁰, L. Gruber⁴⁷,
 B.R. Gruberg Cazon⁶², C. Gu³, M. Guarise²⁰, P. A. Günther¹⁶, E. Gushchin⁴⁰, A. Guth¹³,
 Y. Guz^{43,47}, T. Gys⁴⁷, T. Hadavizadeh⁶⁸, G. Haefeli⁴⁸, C. Haen⁴⁷, J. Haimberger⁴⁷,
 S.C. Haines⁵⁴, T. Halewood-leagas⁵⁹, P.M. Hamilton⁶⁵, Q. Han⁷, X. Han¹⁶, T.H. Hancock⁶²,
 S. Hansmann-Menzemer¹⁶, N. Harnew⁶², T. Harrison⁵⁹, C. Hasse⁴⁷, M. Hatch⁴⁷, J. He⁵,
 M. Hecker⁶⁰, K. Heijhoff³¹, K. Heinicke¹⁴, A.M. Hennequin⁴⁷, K. Hennessy⁵⁹, L. Henry^{25,46},
 J. Heuel¹³, A. Hicheur², D. Hill⁶², M. Hilton⁶¹, S.E. Hollitt¹⁴, P.H. Hopchev⁴⁸, J. Hu¹⁶, J. Hu⁷¹,
 W. Hu⁷, W. Huang⁵, X. Huang⁷², W. Hulsbergen³¹, R.J. Hunter⁵⁵, M. Hushchyn⁸¹,
 D. Hutchcroft⁵⁹, D. Hynds³¹, P. Ibis¹⁴, M. Idzik³⁴, D. Ilin³⁷, P. Ilten⁵², A. Inglese³⁷,
 A. Ishteev⁸⁰, K. Ivshin³⁷, R. Jacobsson⁴⁷, S. Jakobsen⁴⁷, E. Jans³¹, B.K. Jashal⁴⁶,
 A. Jawahery⁶⁵, V. Jevtic¹⁴, M. Jezabek³³, F. Jiang³, M. John⁶², D. Johnson⁴⁷, C.R. Jones⁵⁴,
 T.P. Jones⁵⁵, B. Jost⁴⁷, N. Jurik⁴⁷, S. Kandybei⁵⁰, Y. Kang³, M. Karacson⁴⁷, J.M. Kariuki⁵³,
 N. Kazeev⁸¹, M. Kecke¹⁶, F. Keizer^{54,47}, M. Kenzie⁵⁵, T. Ketel³², B. Khanji⁴⁷, A. Kharisova⁸²,
 S. Kholodenko⁴³, K.E. Kim⁶⁷, T. Kirn¹³, V.S. Kirsebom⁴⁸, O. Kitouni⁶³, S. Klaver³¹,
 K. Klimaszewski³⁵, S. Koliiev⁵¹, A. Kondybayeva⁸⁰, A. Konoplyannikov³⁸, P. Kopciwicz³⁴,
 R. Kopecna¹⁶, P. Koppenburg³¹, M. Korolev³⁹, I. Kostiuk^{31,51}, O. Kot⁵¹, S. Kotriakhova^{37,30},
 P. Kravchenko³⁷, L. Kravchuk⁴⁰, R.D. Krawczyk⁴⁷, M. Kreps⁵⁵, F. Kress⁶⁰, S. Kretschmar¹³,
 P. Krokovny^{42,v}, W. Krupa³⁴, W. Krzemien³⁵, W. Kucewicz^{33,l}, M. Kucharczyk³³,
 V. Kudryavtsev^{42,v}, H.S. Kuindersma³¹, G.J. Kunde⁶⁶, T. Kvaratskheliya³⁸, D. Lacarrere⁴⁷,
 G. Lafferty⁶¹, A. Lai²⁶, A. Lampis²⁶, D. Lancierini⁴⁹, J.J. Lane⁶¹, R. Lane⁵³, G. Lanfranchi²²,
 C. Langenbruch¹³, J. Langer¹⁴, O. Lantwin^{49,80}, T. Latham⁵⁵, F. Lazzari^{28,t}, R. Le Gac¹⁰,
 S.H. Lee⁸⁴, R. Lefèvre⁹, A. Leflat³⁹, S. Legotin⁸⁰, O. Leroy¹⁰, T. Lesiak³³, B. Leverington¹⁶,
 H. Li⁷¹, L. Li⁶², P. Li¹⁶, X. Li⁶⁶, Y. Li⁶, Y. Li⁶, Z. Li⁶⁷, X. Liang⁶⁷, T. Lin⁶⁰, R. Lindner⁴⁷,
 V. Lisovskyi¹⁴, R. Litvinov²⁶, G. Liu⁷¹, H. Liu⁵, S. Liu⁶, X. Liu³, A. Loi²⁶, J. Lomba Castro⁴⁵,
 I. Longstaff⁵⁸, J.H. Lopes², G. Loustau⁴⁹, G.H. Lovell⁵⁴, Y. Lu⁶, D. Lucchesi^{27,m}, S. Luchuk⁴⁰,
 M. Lucio Martinez³¹, V. Lukashenko³¹, Y. Luo³, A. Lupato⁶¹, E. Luppi^{20,g}, O. Lupton⁵⁵,
 A. Lusiani^{28,r}, X. Lyu⁵, L. Ma⁶, S. Maccolini^{19,e}, F. Machefer¹¹, F. Maciuc³⁶, V. Macko⁴⁸,
 P. Mackowiak¹⁴, S. Maddrell-Mander⁵³, O. Madejczyk³⁴, L.R. Madhan Mohan⁵³, O. Maev³⁷,
 A. Maevskiy⁸¹, D. Maisuzenko³⁷, M.W. Majewski³⁴, S. Malde⁶², B. Malecki⁴⁷, A. Malinin⁷⁹,
 T. Maltsev^{42,v}, H. Malygina¹⁶, G. Manca^{26,f}, G. Mancinelli¹⁰, R. Manera Escalero⁴⁴,
 D. Manuzzi^{19,e}, D. Marangotto^{25,o}, J. Maratas^{9,u}, J.F. Marchand⁸, U. Marconi¹⁹,
 S. Mariani^{21,47,h}, C. Marin Benito¹¹, M. Marinangeli⁴⁸, P. Marino⁴⁸, J. Marks¹⁶, P.J. Marshall⁵⁹,
 G. Martellotti³⁰, L. Martinazzoli⁴⁷, M. Martinelli^{24,j}, D. Martinez Santos⁴⁵, F. Martinez Vidal⁴⁶,
 A. Massafferri¹, M. Materok¹³, R. Matev⁴⁷, A. Mathad⁴⁹, Z. Mathe⁴⁷, V. Matiunin³⁸,
 C. Matteuzzi²⁴, K.R. Mattioli⁸⁴, A. Mauri³¹, E. Maurice^{11,b}, J. Mauricio⁴⁴, M. Mazurek³⁵,
 M. McCann⁶⁰, L. McConnell¹⁷, T.H. Mcgrath⁶¹, A. McNab⁶¹, R. McNulty¹⁷, J.V. Mead⁵⁹,
 B. Meadows⁶⁴, C. Meaux¹⁰, G. Meier¹⁴, N. Meinert⁷⁵, D. Melnychuk³⁵, S. Meloni^{24,j},
 M. Merk^{31,78}, A. Merli²⁵, L. Meyer Garcia², M. Mikhasenko⁴⁷, D.A. Milanes⁷³, E. Millard⁵⁵,

M. Milovanovic⁴⁷, M.-N. Minard⁸, L. Minzoni^{20,g}, S.E. Mitchell⁵⁷, B. Mitreska⁶¹, D.S. Mitzel⁴⁷,
A. Mödden¹⁴, R.A. Mohammed⁶², R.D. Moise⁶⁰, T. Mombächer¹⁴, I.A. Monroy⁷³, S. Monteil⁹,
M. Morandin²⁷, G. Morello²², M.J. Morello^{28,r}, J. Moron³⁴, A.B. Morris⁷⁴, A.G. Morris⁵⁵,
R. Mountain⁶⁷, H. Mu³, F. Muheim⁵⁷, M. Mukherjee⁷, M. Mulder⁴⁷, D. Müller⁴⁷, K. Müller⁴⁹,
C.H. Murphy⁶², D. Murray⁶¹, P. Muzzetto²⁶, P. Naik⁵³, T. Nakada⁴⁸, R. Nandakumar⁵⁶,
T. Nanut⁴⁸, I. Nasteva², M. Needham⁵⁷, I. Neri^{20,g}, N. Neri^{25,o}, S. Neubert⁷⁴, N. Neufeld⁴⁷,
R. Newcombe⁶⁰, T.D. Nguyen⁴⁸, C. Nguyen-Mau⁴⁸, E.M. Niel¹¹, S. Nieswand¹³, N. Nikitin³⁹,
N.S. Nolte⁴⁷, C. Nunez⁸⁴, A. Oblakowska-Mucha³⁴, V. Obraztsov⁴³, D.P. O'Hanlon⁵³,
R. Oldeman^{26,f}, C.J.G. Onderwater⁷⁷, A. Ossowska³³, J.M. Otalora Goicochea²,
T. Ovsiannikova³⁸, P. Owen⁴⁹, A. Oyanguren⁴⁶, B. Pagare⁵⁵, P.R. Pais⁴⁷, T. Pajero^{28,47,r},
A. Palano¹⁸, M. Palutan²², Y. Pan⁶¹, G. Panshin⁸², A. Papanestis⁵⁶, M. Pappagallo^{18,d},
L.L. Pappalardo^{20,g}, C. Pappenheimer⁶⁴, W. Parker⁶⁵, C. Parkes⁶¹, C.J. Parkinson⁴⁵,
B. Passalacqua²⁰, G. Passaleva²¹, A. Pastore¹⁸, M. Patel⁶⁰, C. Patrignani^{19,e}, C.J. Pawley⁷⁸,
A. Pearce⁴⁷, A. Pellegrino³¹, M. Pepe Altarelli⁴⁷, S. Perazzini¹⁹, D. Pereima³⁸, P. Perret⁹,
K. Petridis⁵³, A. Petrolini^{23,i}, A. Petrov⁷⁹, S. Petrucci⁵⁷, M. Petruzzo²⁵, A. Philippov⁴¹,
L. Pica²⁸, M. Piccini⁷⁶, B. Pietrzyk⁸, G. Pietrzyk⁴⁸, M. Pili⁶², D. Pinci³⁰, J. Pinzino⁴⁷,
F. Pisani⁴⁷, A. Piucci¹⁶, Resmi P.K¹⁰, V. Placinta³⁶, S. Playfer⁵⁷, J. Plews⁵², M. Plo Casasus⁴⁵,
F. Polci¹², M. Poli Lener²², M. Poliakov⁶⁷, A. Poluektov¹⁰, N. Polukhina^{80,c}, I. Polyakov⁶⁷,
E. Polycarpo², G.J. Pomery⁵³, S. Ponce⁴⁷, A. Popov⁴³, D. Popov^{5,47}, S. Popov⁴¹,
S. Poslavskii⁴³, K. Prasanth³³, L. Promberger⁴⁷, C. Prouve⁴⁵, V. Pugatch⁵¹, A. Puig Navarro⁴⁹,
H. Pullen⁶², G. Punzi^{28,n}, W. Qian⁵, J. Qin⁵, R. Quagliani¹², B. Quintana⁸, N.V. Raab¹⁷,
R.I. Rabadan Trejo¹⁰, B. Rachwal³⁴, J.H. Rademacker⁵³, M. Rama²⁸, M. Ramos Pernas⁵⁵,
M.S. Rangel², F. Ratnikov^{41,81}, G. Raven³², M. Reboud⁸, F. Redi⁴⁸, F. Reiss¹²,
C. Remon Alepuz⁴⁶, Z. Ren³, V. Renaudin⁶², R. Ribatti²⁸, S. Ricciardi⁵⁶, D.S. Richards⁵⁶,
K. Rinnert⁵⁹, P. Robbe¹¹, A. Robert¹², G. Robertson⁵⁷, A.B. Rodrigues⁴⁸, E. Rodrigues⁵⁹,
J.A. Rodriguez Lopez⁷³, A. Rollings⁶², P. Roloff⁴⁷, V. Romanovskiy⁴³, M. Romero Lamas⁴⁵,
A. Romero Vidal⁴⁵, J.D. Roth⁸⁴, M. Rotondo²², M.S. Rudolph⁶⁷, T. Ruf⁴⁷, J. Ruiz Vidal⁴⁶,
A. Ryzhikov⁸¹, J. Ryzka³⁴, J.J. Saborido Silva⁴⁵, N. Sagidova³⁷, N. Sahoo⁵⁵, B. Saitta^{26,f},
D. Sanchez Gonzalo⁴⁴, C. Sanchez Gras³¹, C. Sanchez Mayordomo⁴⁶, R. Santacesaria³⁰,
C. Santamarina Rios⁴⁵, M. Santimaria²², E. Santovetti^{29,k}, D. Saranin⁸⁰, G. Sarpis⁶¹,
M. Sarpis⁷⁴, A. Sarti³⁰, C. Satriano^{30,q}, A. Satta²⁹, M. Saur⁵, D. Savrina^{38,39}, H. Sazak⁹,
L.G. Scantlebury Smead⁶², S. Schael¹³, M. Schellenberg¹⁴, M. Schiller⁵⁸, H. Schindler⁴⁷,
M. Schmelling¹⁵, T. Schmelzer¹⁴, B. Schmidt⁴⁷, O. Schneider⁴⁸, A. Schopper⁴⁷, M. Schubiger³¹,
S. Schulte⁴⁸, M.H. Schune¹¹, R. Schwemmer⁴⁷, B. Sciascia²², A. Sciubba³⁰, S. Sellam⁴⁵,
A. Semennikov³⁸, M. Senghi Soares³², A. Sergi^{52,47}, N. Serra⁴⁹, J. Serrano¹⁰, L. Sestini²⁷,
A. Seuthe¹⁴, P. Seyfert⁴⁷, D.M. Shangase⁸⁴, M. Shapkin⁴³, I. Shchemerov⁸⁰, L. Shchutska⁴⁸,
T. Shears⁵⁹, L. Shekhtman^{42,v}, Z. Shen⁴, V. Shevchenko⁷⁹, E.B. Shields^{24,j}, E. Shmanin⁸⁰,
J.D. Shupperd⁶⁷, B.G. Siddi²⁰, R. Silva Coutinho⁴⁹, G. Simi²⁷, S. Simone^{18,d}, I. Skiba^{20,g},
N. Skidmore⁷⁴, T. Skwarnicki⁶⁷, M.W. Slater⁵², J.C. Smallwood⁶², J.G. Smeaton⁵⁴,
A. Smetkina³⁸, E. Smith¹³, M. Smith⁶⁰, A. Snoch³¹, M. Soares¹⁹, L. Soares Lavra⁹,
M.D. Sokoloff⁶⁴, F.J.P. Soler⁵⁸, A. Solovov³⁷, I. Solovyevev³⁷, F.L. Souza De Almeida²,
B. Souza De Paula², B. Spaan¹⁴, E. Spadaro Norella^{25,o}, P. Spradlin⁵⁸, F. Stagni⁴⁷, M. Stahl⁶⁴,
S. Stahl⁴⁷, P. Stefko⁴⁸, O. Steinkamp^{49,80}, S. Stemmler¹⁶, O. Stenyakin⁴³, H. Stevens¹⁴,
S. Stone⁶⁷, M.E. Stramaglia⁴⁸, M. Straticiu³⁶, D. Strelakina⁸⁰, S. Strokov⁸², F. Suljik⁶²,
J. Sun²⁶, L. Sun⁷², Y. Sun⁶⁵, P. Svihra⁶¹, P.N. Swallow⁵², K. Swientek³⁴, A. Szabelski³⁵,
T. Szumlak³⁴, M. Szymanski⁴⁷, S. Taneja⁶¹, Z. Tang³, T. Tekampe¹⁴, F. Teubert⁴⁷,
E. Thomas⁴⁷, K.A. Thomson⁵⁹, M.J. Tilley⁶⁰, V. Tisserand⁹, S. T'Jampens⁸, M. Tobin⁶,
S. Tolk⁴⁷, L. Tomassetti^{20,g}, D. Torres Machado¹, D.Y. Tou¹², M. Traill⁵⁸, M.T. Tran⁴⁸,
E. Trifonova⁸⁰, C. Trippel⁴⁸, A. Tsaregorodtsev¹⁰, G. Tuci^{28,n}, A. Tully⁴⁸, N. Tuning³¹,
A. Ukleja³⁵, D.J. Unverzagt¹⁶, A. Usachov³¹, A. Ustyuzhanin^{41,81}, U. Uwer¹⁶, A. Vagner⁸²,

V. Vagnoni¹⁹, A. Valassi⁴⁷, G. Valenti¹⁹, N. Valls Canudas⁴⁴, M. van Beuzekom³¹,
H. Van Hecke⁶⁶, E. van Herwijnen⁸⁰, C.B. Van Hulse¹⁷, M. van Veghel⁷⁷, R. Vazquez Gomez⁴⁵,
P. Vazquez Regueiro⁴⁵, C. Vázquez Sierra³¹, S. Vecchi²⁰, J.J. Velthuis⁵³, M. Veltri^{21,p},
A. Venkateswaran⁶⁷, M. Veronesi³¹, M. Vesterinen⁵⁵, D. Vieira⁶⁴, M. Vieites Diaz⁴⁸,
H. Viemann⁷⁵, X. Vilasis-Cardona⁸³, E. Vilella Figueras⁵⁹, P. Vincent¹², G. Vitali²⁸,
A. Vollhardt⁴⁹, D. Vom Bruch¹², A. Vorobyev³⁷, V. Vorobyev^{42,v}, N. Voropaev³⁷, R. Waldi⁷⁵,
J. Walsh²⁸, C. Wang¹⁶, J. Wang³, J. Wang⁷², J. Wang⁴, J. Wang⁶, M. Wang³, R. Wang⁵³,
Y. Wang⁷, Z. Wang⁴⁹, D.R. Ward⁵⁴, H.M. Wark⁵⁹, N.K. Watson⁵², S.G. Weber¹²,
D. Websdale⁶⁰, C. Weisser⁶³, B.D.C. Westhenry⁵³, D.J. White⁶¹, M. Whitehead⁵³,
D. Wiedner¹⁴, G. Wilkinson⁶², M. Wilkinson⁶⁷, I. Williams⁵⁴, M. Williams^{63,68},
M.R.J. Williams⁵⁷, F.F. Wilson⁵⁶, W. Wislicki³⁵, M. Witek³³, L. Witola¹⁶, G. Wormser¹¹,
S.A. Wotton⁵⁴, H. Wu⁶⁷, K. Wyllie⁴⁷, Z. Xiang⁵, D. Xiao⁷, Y. Xie⁷, H. Xing⁷¹, A. Xu⁴, J. Xu⁵,
L. Xu³, M. Xu⁷, Q. Xu⁵, Z. Xu⁵, Z. Xu⁴, D. Yang³, Y. Yang⁵, Z. Yang³, Z. Yang⁶⁵, Y. Yao⁶⁷,
L.E. Yeomans⁵⁹, H. Yin⁷, J. Yu⁷⁰, X. Yuan⁶⁷, O. Yushchenko⁴³, K.A. Zarebski⁵²,
M. Zavertyaev^{15,c}, M. Zdybal³³, O. Zenaiev⁴⁷, M. Zeng³, D. Zhang⁷, L. Zhang³, S. Zhang⁴,
Y. Zhang⁴⁷, Y. Zhang⁶², A. Zhelezov¹⁶, Y. Zheng⁵, X. Zhou⁵, Y. Zhou⁵, X. Zhu³,
V. Zhukov^{13,39}, J.B. Zonneveld⁵⁷, S. Zucchelli^{19,c}, D. Zuliani²⁷, G. Zunica⁶¹.

¹Centro Brasileiro de Pesquisas Físicas (CBPF), Rio de Janeiro, Brazil

²Universidade Federal do Rio de Janeiro (UFRJ), Rio de Janeiro, Brazil

³Center for High Energy Physics, Tsinghua University, Beijing, China

⁴School of Physics State Key Laboratory of Nuclear Physics and Technology, Peking University, Beijing, China

⁵University of Chinese Academy of Sciences, Beijing, China

⁶Institute Of High Energy Physics (IHEP), Beijing, China

⁷Institute of Particle Physics, Central China Normal University, Wuhan, Hubei, China

⁸Univ. Grenoble Alpes, Univ. Savoie Mont Blanc, CNRS, IN2P3-LAPP, Annecy, France

⁹Université Clermont Auvergne, CNRS/IN2P3, LPC, Clermont-Ferrand, France

¹⁰Aix Marseille Univ, CNRS/IN2P3, CPPM, Marseille, France

¹¹Ijclab, Orsay, France

¹²LPNHE, Sorbonne Université, Paris Diderot Sorbonne Paris Cité, CNRS/IN2P3, Paris, France

¹³I. Physikalisches Institut, RWTH Aachen University, Aachen, Germany

¹⁴Fakultät Physik, Technische Universität Dortmund, Dortmund, Germany

¹⁵Max-Planck-Institut für Kernphysik (MPIK), Heidelberg, Germany

¹⁶Physikalisches Institut, Ruprecht-Karls-Universität Heidelberg, Heidelberg, Germany

¹⁷School of Physics, University College Dublin, Dublin, Ireland

¹⁸INFN Sezione di Bari, Bari, Italy

¹⁹INFN Sezione di Bologna, Bologna, Italy

²⁰INFN Sezione di Ferrara, Ferrara, Italy

²¹INFN Sezione di Firenze, Firenze, Italy

²²INFN Laboratori Nazionali di Frascati, Frascati, Italy

²³INFN Sezione di Genova, Genova, Italy

²⁴INFN Sezione di Milano-Bicocca, Milano, Italy

²⁵INFN Sezione di Milano, Milano, Italy

²⁶INFN Sezione di Cagliari, Monserrato, Italy

²⁷Università degli Studi di Padova, Università e INFN, Padova, Padova, Italy

²⁸INFN Sezione di Pisa, Pisa, Italy

²⁹INFN Sezione di Roma Tor Vergata, Roma, Italy

³⁰INFN Sezione di Roma La Sapienza, Roma, Italy

³¹Nikhef National Institute for Subatomic Physics, Amsterdam, Netherlands

³²Nikhef National Institute for Subatomic Physics and VU University Amsterdam, Amsterdam, Netherlands

³³Henryk Niewodniczanski Institute of Nuclear Physics Polish Academy of Sciences, Kraków, Poland

³⁴AGH - University of Science and Technology, Faculty of Physics and Applied Computer Science, Kraków, Poland

- ³⁵ *National Center for Nuclear Research (NCBJ), Warsaw, Poland*
- ³⁶ *Horia Hulubei National Institute of Physics and Nuclear Engineering, Bucharest-Magurele, Romania*
- ³⁷ *Petersburg Nuclear Physics Institute NRC Kurchatov Institute (PNPI NRC KI), Gatchina, Russia*
- ³⁸ *Institute of Theoretical and Experimental Physics NRC Kurchatov Institute (ITEP NRC KI), Moscow, Russia*
- ³⁹ *Institute of Nuclear Physics, Moscow State University (SINP MSU), Moscow, Russia*
- ⁴⁰ *Institute for Nuclear Research of the Russian Academy of Sciences (INR RAS), Moscow, Russia*
- ⁴¹ *Yandex School of Data Analysis, Moscow, Russia*
- ⁴² *Budker Institute of Nuclear Physics (SB RAS), Novosibirsk, Russia*
- ⁴³ *Institute for High Energy Physics NRC Kurchatov Institute (IHEP NRC KI), Protvino, Russia, Protvino, Russia*
- ⁴⁴ *ICCUB, Universitat de Barcelona, Barcelona, Spain*
- ⁴⁵ *Instituto Galego de Física de Altas Enerxías (IGFAE), Universidade de Santiago de Compostela, Santiago de Compostela, Spain*
- ⁴⁶ *Instituto de Física Corpuscular, Centro Mixto Universidad de Valencia - CSIC, Valencia, Spain*
- ⁴⁷ *European Organization for Nuclear Research (CERN), Geneva, Switzerland*
- ⁴⁸ *Institute of Physics, Ecole Polytechnique Fédérale de Lausanne (EPFL), Lausanne, Switzerland*
- ⁴⁹ *Physik-Institut, Universität Zürich, Zürich, Switzerland*
- ⁵⁰ *NSC Kharkiv Institute of Physics and Technology (NSC KIPT), Kharkiv, Ukraine*
- ⁵¹ *Institute for Nuclear Research of the National Academy of Sciences (KINR), Kyiv, Ukraine*
- ⁵² *University of Birmingham, Birmingham, United Kingdom*
- ⁵³ *H.H. Wills Physics Laboratory, University of Bristol, Bristol, United Kingdom*
- ⁵⁴ *Cavendish Laboratory, University of Cambridge, Cambridge, United Kingdom*
- ⁵⁵ *Department of Physics, University of Warwick, Coventry, United Kingdom*
- ⁵⁶ *STFC Rutherford Appleton Laboratory, Didcot, United Kingdom*
- ⁵⁷ *School of Physics and Astronomy, University of Edinburgh, Edinburgh, United Kingdom*
- ⁵⁸ *School of Physics and Astronomy, University of Glasgow, Glasgow, United Kingdom*
- ⁵⁹ *Oliver Lodge Laboratory, University of Liverpool, Liverpool, United Kingdom*
- ⁶⁰ *Imperial College London, London, United Kingdom*
- ⁶¹ *Department of Physics and Astronomy, University of Manchester, Manchester, United Kingdom*
- ⁶² *Department of Physics, University of Oxford, Oxford, United Kingdom*
- ⁶³ *Massachusetts Institute of Technology, Cambridge, MA, United States*
- ⁶⁴ *University of Cincinnati, Cincinnati, OH, United States*
- ⁶⁵ *University of Maryland, College Park, MD, United States*
- ⁶⁶ *Los Alamos National Laboratory (LANL), Los Alamos, United States*
- ⁶⁷ *Syracuse University, Syracuse, NY, United States*
- ⁶⁸ *School of Physics and Astronomy, Monash University, Melbourne, Australia, associated to ⁵⁵*
- ⁶⁹ *Pontifícia Universidade Católica do Rio de Janeiro (PUC-Rio), Rio de Janeiro, Brazil, associated to ²*
- ⁷⁰ *Physics and Micro Electronic College, Hunan University, Changsha City, China, associated to ⁷*
- ⁷¹ *Guangdong Provincial Key Laboratory of Nuclear Science, Institute of Quantum Matter, South China Normal University, Guangzhou, China, associated to ³*
- ⁷² *School of Physics and Technology, Wuhan University, Wuhan, China, associated to ³*
- ⁷³ *Departamento de Física, Universidad Nacional de Colombia, Bogota, Colombia, associated to ¹²*
- ⁷⁴ *Universität Bonn - Helmholtz-Institut für Strahlen und Kernphysik, Bonn, Germany, associated to ¹⁶*
- ⁷⁵ *Institut für Physik, Universität Rostock, Rostock, Germany, associated to ¹⁶*
- ⁷⁶ *INFN Sezione di Perugia, Perugia, Italy, associated to ²⁰*
- ⁷⁷ *Van Swinderen Institute, University of Groningen, Groningen, Netherlands, associated to ³¹*
- ⁷⁸ *Universiteit Maastricht, Maastricht, Netherlands, associated to ³¹*
- ⁷⁹ *National Research Centre Kurchatov Institute, Moscow, Russia, associated to ³⁸*
- ⁸⁰ *National University of Science and Technology "MISIS", Moscow, Russia, associated to ³⁸*
- ⁸¹ *National Research University Higher School of Economics, Moscow, Russia, associated to ⁴¹*
- ⁸² *National Research Tomsk Polytechnic University, Tomsk, Russia, associated to ³⁸*
- ⁸³ *DS4DS, La Salle, Universitat Ramon Llull, Barcelona, Spain, associated to ⁴⁴*
- ⁸⁴ *University of Michigan, Ann Arbor, United States, associated to ⁶⁷*

^a *Universidade Federal do Triângulo Mineiro (UFMT), Uberaba-MG, Brazil*

^b *Laboratoire Leprince-Ringuet, Palaiseau, France*

- ^c*P.N. Lebedev Physical Institute, Russian Academy of Science (LPI RAS), Moscow, Russia*
- ^d*Università di Bari, Bari, Italy*
- ^e*Università di Bologna, Bologna, Italy*
- ^f*Università di Cagliari, Cagliari, Italy*
- ^g*Università di Ferrara, Ferrara, Italy*
- ^h*Università di Firenze, Firenze, Italy*
- ⁱ*Università di Genova, Genova, Italy*
- ^j*Università di Milano Bicocca, Milano, Italy*
- ^k*Università di Roma Tor Vergata, Roma, Italy*
- ^l*AGH - University of Science and Technology, Faculty of Computer Science, Electronics and Telecommunications, Kraków, Poland*
- ^m*Università di Padova, Padova, Italy*
- ⁿ*Università di Pisa, Pisa, Italy*
- ^o*Università degli Studi di Milano, Milano, Italy*
- ^p*Università di Urbino, Urbino, Italy*
- ^q*Università della Basilicata, Potenza, Italy*
- ^r*Scuola Normale Superiore, Pisa, Italy*
- ^s*Università di Modena e Reggio Emilia, Modena, Italy*
- ^t*Università di Siena, Siena, Italy*
- ^u*MSU - Iligan Institute of Technology (MSU-IIT), Iligan, Philippines*
- ^v*Novosibirsk State University, Novosibirsk, Russia*
- ^w*INFN Sezione di Trieste, Trieste, Italy*